*sustainability*

MDPI

*Review*

# Mechanical Properties and Durability of Polypropylene and Steel Fiber-Reinforced Recycled Aggregates Concrete (FRRAC): A Review

**Peng Zhang [1], Yonghui Yang [1], Juan Wang [1,*], Shaowei Hu [1,2], Meiju Jiao [1] and Yifeng Ling [3]**

[1] School of Water Conservancy Engineering, Zhengzhou University, Zhengzhou 450001, China; zhangpeng@zzu.edu.cn (P.Z.); yang1287820@163.com (Y.Y.); hushaowei@cqu.edu.cn (S.H.); jiaomj@zzu.edu.cn (M.J.)

[2] College of Civil Engineering, Chongqing University, Chongqing 400045, China

[3] Department of Civil, Construction and Environmental Engineering, Iowa State University, Ames, IA 50011, USA; yling@iastate.edu

* Correspondence: wangjuan@zzu.edu.cn

Received: 7 October 2020; Accepted: 13 November 2020; Published: 15 November 2020




**Abstract:** With the development of concrete engineering, a large amount of construction, demolition, excavation waste (CDEW) has been produced. The treated CDEW can be used as recycled aggregate to replace natural aggregate, which can not only reduce environmental pollution and construction-related resource waste caused by CDEW, but also save natural resources. However, the mechanical properties and durability of Recycled Aggregates Concrete (RAC) are generally worse than that of ordinary concrete. Various fiber or mineral materials are usually used in RAC to improve the mechanical properties and durability of the matrix. In RAC, polypropylene (PP) fiber and steel fiber (SF) are two kinds most commonly used fiber materials, which can enhance the strength and toughness of RAC and compensate the defects of RAC to some extent. In this paper, the literature on PP fiber- and SF-reinforced RAC (FRRAC) is reviewed, with a focus on the consistence, mechanical performance (compressive strength, tensile strength, stress–strain relationship, elastic modulus, and shear strength), durability (water absorption, chloride permeability, carbonation, freeze–thaw cycling, and shrinkage), and microstructure. The research findings regarding FRRAC were analyzed and compared. The results showed that adding mineral additives and fiber in RAC had a good synergistic effect, which made FRRAC have good mechanical properties, high durability and high temperature resistance, and several application prospects. The information and summary presented in this paper exhibit new knowledge and information on the application of FRRAC.

**Keywords:** FRRAC; consistence; mechanical properties; durability

## 1. Introduction

Owing to the limited amount of natural aggregate (NA) resources, the necessity of treating construction, demolition, excavation waste (CDEW) as an aggregate has been recognized in most countries [1]. However, the recycling rate of CDEW in developed countries in Europe was >90%, but for every 100 million tons of construction waste produced, at least 10 million tons of CDEW were unused, so there was a lot of CDEW that was not recycled. In some areas of Japan, the recycling rate was 100%. Until 2012, more than 3 billion tons of CDEW were produced annually worldwide [2]. China produced approximately 3.5 billion tons of construction waste in 2016, with 200 million tons of new construction waste added each year and the utilization rate was only approximately 5% [3].

Simple landfilling or stacking of CDEW not only wastes land resources but also generates a large amount of carbon dioxide and consumes a large amount of energy [4]. CDEW contains a large amount

of calcium silicate hydrate, $Ca(OH)_2$, sulfate ions and heavy metal ions. If they are directly buried in the soil without treatment, they will cause pollution to the soil and water [5]. The benefits of CDEW reuse include the mitigation of CDEW landfilling and dumping problems, reduction in the energy loss in production and transportation of aggregates, and protection of natural resources. Using CDEW as recycled aggregates (Ras) in concrete production can not only reduce environmental pollution and the exploitation amount of natural resources for natural aggregates (NAs), but also be a sustainable development technology. CDEW can be separated, broken and reused as aggregate. CDEW, as recycled aggregate (RA), can be divided into the following three categories: recycled concrete aggregates, recycled masonry aggregates, and mixed recycled aggregate (RA) [6]. Therefore, the use of CDEW in RAC production is a potential viable alternative. In the reuse process, the CDEW is typically crushed to a suitable size and used as an aggregate for concrete. The process of producing RAs using CDEW is shown in Figure 1.

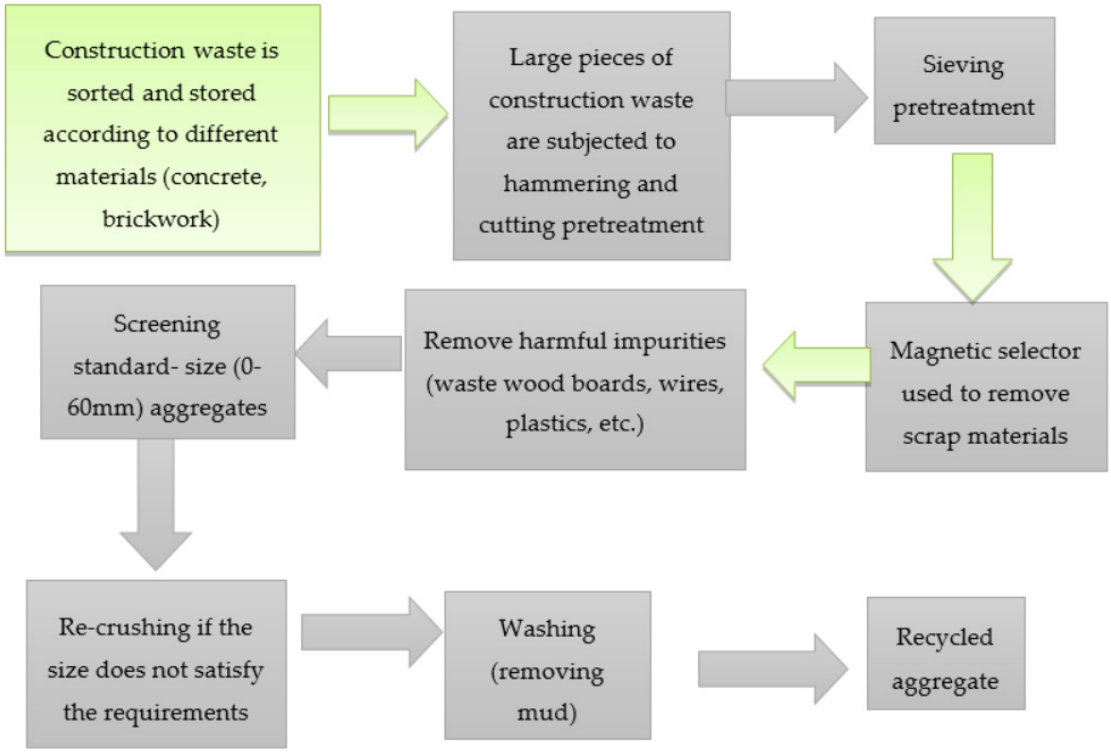



**Figure 1.** Production of recycled aggregates (RAs) using construction, demolition, excavation waste (CDEW) [7,8].

Compared with NAs, RAs are typically characterized by high water absorption, high porosity, lower strength and stiffness, larger creep and shrinkage, and a lower apparent density owing to the presence of weak particles such as old mortar blocks [9,10]. Although the performance of RAs is inferior to that of NAs, RAs are eco-friendly building materials with considerable application value. When the proportion of RA replacing NA is <30%, the replacement has little influence on some properties of the concrete, such as the tensile strength, compressive strength, chloride-ion corrosion, and carbonation. However, the compressive strength of the matrix decreases with an increase in the RA content [11–15].

When the aggregate in the matrix is completely replaced with RA, the decrease in the matrix compressive strength is three times that of when the RA content is 50% [16]. Under the same conditions, the matrix flexural tensile strength decreases by 10–13% compared with that of the reference concrete [17]. This may have been due to old mortar affiliated with the RA. There are many pores and cracks in the old mortar, which increase the water consumption of the matrix. However, Rao et al. [18] reported that the amount of RA in the matrix had insignificant effects on the bending strength and

tensile strength of the matrix. The stress–strain curve and the peak value of the stress under the axial load of recycled coarse aggregate (RCA) concrete are similar to those for natural aggregate concrete (NAC). The strain increases with the RA content, and the elastic modulus and ductility are lower than those of NAC [19,20]. Gowda et al. [21] discovered that the compressive strength and rigidity of RCA concrete are similar to those of ordinary concrete in the temperature range of 25–800 °C. Gales et al. [22] reported that when the matrix was in a 500 °C environment and the RA content increased, the residual strength and elastic modulus of the matrix gradually decreased. This indicates that RAC has resistance to high temperature.

There is an interfacial transition zone (ITZ) in concrete, which significantly affects the mechanical properties and durability of the concrete. There are five main types of ITZs in RAC: (1) ITZs formed by new mortar and new aggregate (NA); (2) ITZs formed by new mortar and old aggregate; (3) ITZs formed by old mortar and new mortar; (4) ITZs formed by old mortar and RA; (5) ITZs formed by old mortar and NA [23,24]. The ITZ for RAC is shown in Figure 2. The ITZs are weaknesses in cement-based composite materials [25]. The ITZ of concrete, which usually has more cracks and holes, is the weakest part of concrete. Under the same conditions, RAC has weaker and more complex ITZs than ordinary concrete. This is the main microstructural difference between RAC and ordinary concrete. It is also the fundamental reason why the macroscopic material and structure performance of RAC is worse than that of ordinary concrete. Many scholars have performed in-depth research on ITZ. Poon et al. [26] examined the microstructure of the matrix using scanning electron microscopy (SEM) and concluded that the ITZ areas of RA had lower compactness, and were more porous, as well as more cracks, than those of the benchmark concrete. They also discovered that the microstructure of the RAC significantly affected the RAC performance.

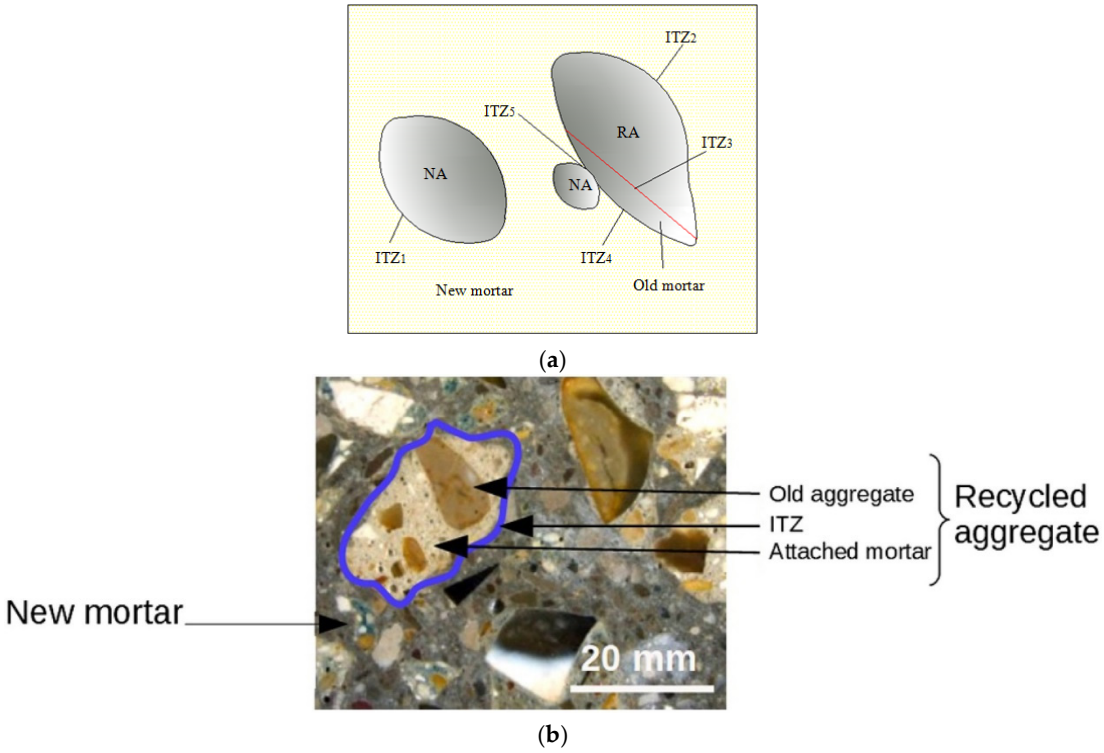



**Figure 2.** Interfacial transition zone (ITZ) for RAC [23,24]. (**a**) Five different ITZs; (**b**) ITZs formed by new mortar and RA.

CDEW is used as an RA, which contains asphalt, glass and other impurities, and these impurities also reduce the performance of RA. In order to remove these impurities, the recycling process of RA needs to be optimized. At the same time, the content of asphalt, glass and asphalt should be

restricted <1%. The sulfate content in RA is generally <2%, and the chloride content <1%, alkali content less than 3.5 kg/m$^3$, thus reducing the chemical impurities in RA and improving the performance of RA [6]. Although, the strength of an RA is lower than that of an NA, the RA surface is rough and porous, which enhances the mechanical bite force between RA and the matrix and improves the strength and surface wear resistance of the matrix [27]. Carneiro et al. [28] reported that the matrix strength with an RA ratio of 25% was higher than that of ordinary concrete. The irregular surface of RA strengthens the physical bond with the matrix. Additionally, RA has strong adhesion with the matrix owing to the hydration reaction [29]. Some mechanical properties of RAC may not be as good as ordinary concrete, but these properties are sufficient for some practical applications of concrete structures [19]. Thus far, RAC has been used in sidewalks and construction of structures in China, and satisfactory results have been obtained. The recycling technology and related standards of CDEW have also gradually matured, and CDEW used as RA is also gradually applied in the structure, pavement, cladding and other building finishes of civil engineering [30]. Thus, RAs have bright application potential.

Adding appropriate mineral additives to RAC can improve the mechanical properties and durability of RAC [31]. An appropriate amount of PP fiber, steel fibers (SFs), blast fiber and glass fiber was added to improve the compressive strength, flexural strength and splitting tensile strength of RAC [4]. In addition, as with traditional concrete, RAC exhibits low bending toughness and fracture toughness. As a result, many kinds of fibers are usually used in traditional concrete and RAC to improve the durability and toughness of the matrix [32–34]. In RAC, polypropylene (PP) fiber and SFs are two of the most commonly used kinds of fiber materials, which can enhance the mechanical properties, durability and toughness of RAC, and make up for the defects of RAC to some extent [35,36].

Ahmed and Lim [4] reviewed the effects of SF, PP fiber, basalt fiber and glass fiber dosage on the compressive strength, splitting tensile strength and flexural strength of RAC in detail, and they also analyzed and suggested the optimal dosage of each fiber. However, the literature review on the effects of high temperature conditions on the compressive strength, splitting tensile strength and flexural strength of RAC reinforced with SF and PP fibers containing mineral additives is helpful for understanding the properties of FRRAC. The relationship between the splitting tensile strength, flexural strength and elastic modulus of FRRAC and compressive strength of FRRAC is necessary to be reviewed. Moreover, the influence of SF and PP fiber content on slump, durability and microstructure performance of RAC has not been reviewed till now. Therefore, the above-mentioned research achievements on FRRAC have been reviewed in this paper. Furthermore, the effects of SF or PP fiber content on elastic modulus, stress–strain, chloride ion permeability, freeze–thawing resistance, carbonization resistance, shrinkage performance, microstructure of RAC were also innovatively analyzed in this work.

The producing process of RA using CDEW and the performance of fiber-reinforced RAC (FRRAC) have been extensively studied. FRRAC preparation technology is diversified; thus, the prepared FRRAC exhibits satisfactory performance and has been used in practical applications. In this study, the influence of fly ash (FA), silica fume, ground granulated blast furnace slag (GGBS), rice husk ash (RHA) and metakaolin (MK) on the compressive strength and splitting tensile strength of RAC, as well as the replacement rate of mineral additives, is analyzed. To obtain a deeper understanding of the performance of FRRAC, this paper analyzes and summarizes the research results regarding the working performance, mechanical properties (compressive strength, splitting tensile strength, flexural strength, elastic modulus and stress–strain), durability, microstructure, and mechanical properties at high temperature of RAC. A method for improving the performance of FRRAC is analyzed to provide a reference for in-depth analysis of FRRAC, and the technical problems faced by FRRAC are also presented.

## 2. Fabrication of FRRAC

### *2.1. Probable Source Materials*

Industrial production is generating increasing amounts of waste, e.g., FA, GGBS, silica fume. The failure to reuse these materials will cause resource wastage and environmental pollution. FA, GGBS, RHA, and silica fume mainly contain $SiO_2$ and $Al_2O_3$. The properties of mostly used cement, RHA, FA, GGBFS, and silica fume are presented in Table 1. $SiO_2$ and $Al_2O_3$ in the concrete matrix can chemically react with $Ca(OH)_2$ and other alkaline compounds to generate hydration products such as tobermorite gel (C-S-H), calcium aluminate hydrate (C2ASH8), tetracalcium aluminate hydrate (C4AH13), and tricalum aluminate hydrate (C3AH6). Due to the silica fume's small particle sizes, the substance can fill pores in the concrete. As indicated by Table 1, the content of $SiO_2$ in silica fume is the highest, and volcanic ash effect are better than other minerals. These materials have a lower specific weight than cement and are ideal for the formation of light and high strength RAC.

**Table 1.** Properties of cement, rice husk ash (RHA), fly ash (FA), ground granulated blast furnace slag (GGBS), and silica fume.

| Ref. | Item | Chemical Composition (Mass%) | | | | | | Specific Gravity ($g/cm^3$) | Specific Surface Area ($cm^2/g$) |
|---|---|---|---|---|---|---|---|---|---|
| | | $SiO_2$ | $Al_2O_3$ | $Fe_2O_3$ | CaO | MgO | $SO_2$ | | |
| Kou and Poon et al. [37] | Cement | 21.0 | 5.9 | 3.4 | 64.7 | 0.9 | 2.6 | 3.15 | 3520 |
| | FA | 56.79 | 28.21 | 5.31 | <3 | 5.21 | 0.68 | 2.31 | 3960 |
| Rattanachu et al. [38] | RHA | 93.5 | 0.2 | 0.4 | 0.9 | 0.4 | 0.2 | - | - |
| Majhi et al. [39] | GGBFS | 38 | 17 | 3 | 29 | 29 | - | 2.82 | - |
| Nuaklong et al. [40] | Silica fume | 85–95 | 0.5–1.7 | 0.4–2 | - | 0.1–0.9 | - | 2.21 | 14,000 |

Tables 2–6 present the effects of the FA, RHA, silica fume, GGBS, and MK contents on the mechanical properties of RAC. As is shown, the addition of silica fume and MK can improve the mechanical properties of the matrix. The MK content is generally approximately 10%, and the MK improves the mechanical properties and durability of the matrix. In particular, increasing the content of MK can result in higher strengths not only in NA geopolymer concrete but also in geopolymer concrete containing RCAs [40]. The activation property of RHA is low, possibly because of its impurities. The effects of GGBS and FA on the improvement of the mechanical properties of the substrate is not very large, but the appropriate amount of incorporation can improve the durability of the substrate, particularly the resistance to chloride ion attack. The control group in each experiment was different, but these minerals also play a role. The FA content is generally approximately 20–30%, however, because of its low ash effect, the output is not easy to be too high. As the age of the base matrix increases, the enhancement effects of GGBS, FA, and RHA on RAC increase. Silica fume's volcanic ash has a better effect than other minerals, but as the cost is higher, it is difficult to add large amounts. Adding these minerals to the matrix can also reduce the amount of cement, thereby reducing carbon dioxide emissions and enabling the recycling of resources. The chemical reaction equations of the matrix when it is attacked by sulphuric acid are as follows [41]:

$$Ca(OH)_2 + H_2SO_4 \rightarrow CaSO_4 \cdot 2H_2O \quad (1)$$

$$3CaO \cdot Al_2O_3 \cdot 12H_2O + 3(CaSO_4 \cdot 2H_2O) + 14H_2O \rightarrow 3CaO \cdot Al_2O_3 \cdot 3CaSO_4 \cdot 32H_2O \quad (2)$$

$$CaO \cdot SiO_2 \cdot 2H_2O + 2H_2SO_4 \rightarrow CaSO_4 + Si(OH)_4 + H_2O \quad (3)$$

The chemical reaction of gypsum with calcium aluminate hydrate (C3A) to produce ettringite is expressed by Equation (2). The volume of calcium aluminate hydrate produced by this reaction is 2–7 times that of the raw material. The increase in the volume of the material inside the matrix increases the internal pressure of the concrete, degrading the performance of the concrete. This is consistent with a study on the use of silica fume, FA, etc. to improve the acid resistance of the matrix [41]. The active

substances of mineral materials, such as $SiO_2$ and $Al_2O_3$, react with calcium hydroxide in the matrix. The hydration calcium aluminum, calcium sulphoaluminate hydrate crystals and secondary C-S-H gel can enhance the strength and durability of the matrix. Studies have indicated that the particle size of silica fume and MK is significantly smaller than that of cement. The pore filling effect of these materials may be the same as that of their hydration in improving matrix compactness.

$$Al_2O_3 \cdot 2SiO_2 \cdot 2H_2O \xrightarrow[\text{Temperature}]{600 \sim 900\ ^\circ C} Al_2O_3 \cdot 2SiO_2 + 2H_2O. \quad (4)$$

**Table 2.** Mechanical properties of RAC with different FA contents.

| Ref. | RA | FA (%) | w/b (Water to Binder) | Compressive Strength (MPa) | Splitting Tensile Strength (MPa) |
|---|---|---|---|---|---|
| Kou and Poon et al. [37] | 100% RCA | 0 | 0.55 | 52.2 | 4.41 |
| | 100% RCA | 25 | 0.55 | 59.1 | 4.49 |
| | 100% RCA | 35 | 0.55 | 56.3 | 3.91 |
| | 100% RCA | 55 | 0.55 | 49.4 | 3.41 |
| Ali et al. [42] | 100% RCA | 0 | 0.5 | 32.60 | 2.29 |
| | 100% RCA | 20 | 0.5 | 31.31 | 2.49 |
| Kim et al. [43] | 100% RCA | 0 | 0.35 | 33 | 2.6 |
| | 100% RCA | 30 | 0.35 | 29 | 2.8 |

**Table 3.** Mechanical properties of RAC with different RHA contents.

| Ref. | RA | RHA (%) | w/b | Compressive Strength (MPa) | Splitting Tensile Strength (MPa) |
|---|---|---|---|---|---|
| Padhi et al. [44] | 100% RCA | 0 | 0.45 | 32.47 | 2.2 |
| | 100% RCA | 10 | 0.45 | 30.39 | 2.12 |
| | 100% RCA | 20 | 0.45 | 24.39 | 1.86 |
| Rattanachu et al. [38] | 100% RA | 0 | 0.45 | 38.4 | - |
| | 100% RA | 20 | 0.45 | 38.3 | - |
| | 100% RA | 35 | 0.45 | 34.4 | - |
| | 100% RA | 50 | 0.45 | 27.0 | - |
| Tangchirpat et al. [45] | 100% RA | 0 | 0.48 | 36.02 | - |
| | 100% RA | 20 | 0.48 | 38.5 | - |
| | 100% RA | 35 | 0.48 | 37.2 | - |
| | 100% RA | 50 | 0.48 | 33.9 | - |
| Alnahhal et al. [46] | 100% RCA | 0 | 0.55 | 35.8 | - |
| | 100% RCA | 10 | 0.55 | 38.9 | - |
| | 100% RCA | 20 | 0.55 | 37.0 | - |
| | 100% RCA | 30 | 0.55 | 33.3 | - |

For the RAC containing GGBS, FA, RHA, MK and silica fume, hydration reaction occurs in the cementitious matrix to generate C-S-H, which can fill the pores inside the matrix and improve the performance of RAC. Although the current using of GGBS, FA, RHA, MK and silica fume in RAC has obtained certain achievements for the recycling industry, the amount of the cement replaced with these industrial waste materials is not up to the standards in existing codes. Therefore, how to replace larger amounts of cement by the industrial waste materials and improve the mechanical properties and durability of RAC at the same time is also a challenging and worthy study area.

**Table 4.** Mechanical properties of RAC with different silica-fume contents.

| Ref. | RA | Silica Fume (%) | w/b | Compressive Strength (MPa) | Splitting Tensile Strength (MPa) |
|---|---|---|---|---|---|
| Corinaldesi et al. [47] | 100% RCA | 0 | 0.4 | 28.41 | - |
| | 100% RCA | 15 | 0.4 | 42.62 | - |
| Koua et al. [48] | 100% RCA | 0 | 0.5 | 48.96 | 3.14 |
| | 100% RCA | 10 | 0.5 | 54.53 | 3.84 |
| Çakır et al. [49] | 100% RCA | 0 | 0.5 | 48.6 | 3.4 |
| | 100% RCA | 5 | 0.5 | 46.4 | 3.4 |
| | 100% RCA | 10 | 0.5 | 48.6 | 3.5 |
| Pedro et al. [50] | 100% RA | 0 | 0.29 | 90.1 | 3.6 |
| | 100% RA | 5 | 0.29 | 93.7 | 3.83 |
| | 100% RA | 10 | 0.29 | 97.3 | 3.87 |

**Table 5.** Mechanical properties of RAC with different GGBS contents.

| Ref. | RA | GGBS (%) | w/b | Compressive Strength (MPa) | Splitting Tensile Strength (MPa) |
|---|---|---|---|---|---|
| Majhi et al. [51] | 100% RCA | 0 | 0.5 | 30.59 | 2.80 |
| | 100% RCA | 20 | 0.5 | 28.16 | 2.65 |
| | 100% RCA | 40 | 0.5 | 26.62 | 2.55 |
| | 100% RCA | 60 | 0.5 | 24.04 | 2.35 |
| Majhi et al. [39] | 100% RCA | 0 | 0.57 | 24.00 | 3.08 |
| | 100% RCA | 60 | 0.57 | 18.42 | 2.7 |
| Majhi et al. [52] | 100% RCA | 0 | 0.58 | 39.04 | - |
| | 100% RCA | 40 | 0.58 | 37.61 | - |
| | 100% RCA | 60 | 0.58 | 32.12 | - |

**Table 6.** Mechanical properties of RAC with different metakaolin (MK) contents.

| Ref. | RC | MK | w/b | Compressive Strength (MPa) | Splitting Tensile Strength (MPa) |
|---|---|---|---|---|---|
| Muduli et al. [53] | 100% RCA | 0 | 0.43 | 32.75 | 2.64 |
| | 100% RCA | 5 | 0.43 | 33.79 | 2.78 |
| | 100% RCA | 10 | 0.43 | 36.27 | 2.91 |
| | 100% RCA | 15 | 0.43 | 38.09 | 3.08 |
| | 100% RCA | 20 | 0.43 | 35.36 | 2.9 |
| Xie et al. [54] | 100% RCA | 0 | 0.55 | 36.1 | - |
| | 100% RCA | 3 | 0.55 | 42.9 | - |
| | 100% RCA | 5 | 0.55 | 44.8 | - |
| | 100% RCA | 7 | 0.55 | 45.9 | - |
| Nuaklong et al. [40] | 100% RCA | 0 | - | 35.2 | 2.9 |
| | 100% RCA | 10 | - | 45 | 4.1 |
| | 100% RCA | 20 | - | 50.6 | 4.4 |
| | 100% RCA | 30 | - | 58.6 | 5.4 |

Note: MK is an anhydrous aluminum silicate ($A1_2O_3 \bullet 2SiO_2 \bullet 2H_2O$, AS2H2) formed by dehydration from kaolin ($A1_2O_3 \bullet 2SiO_2$, AS2) at an appropriate temperature (600~900 °C).

## 2.2. Consistence of Fresh RAC

Compared to NAs, RAs have a rougher surface, a larger angular effect, larger voids, greater water absorption, lower apparent densities, and a higher wear capacity [55]. Therefore, RCAs affect the concrete consistence. When the water/binder (w/b) ratio of self-compacting concrete (SCC) was 0.4 and

the RCA content ranged from 0 to 100%, the slump decreased by 13.4%, reducing the consistence [56]. To achieve the same performance, concrete with 50–100% RAC requires 0.15–0.37% more water than NAC [57]. The high water-absorption rate of the RA reduces the amount of free water in the RCA, and the slump decreases with an increase in the amount of RA.

Additionally, PP fibers and SFs have been added to RAC to reduce its consistence. Matar and Assaad [58] found that when PP fibers (having 12 mm long and 150 aspect ratio) were used with an RCA, the downward trend of the RAC decreases with increasing PP fiber content. This may be due to the adhesive interface between the PP fibers and the matrix; the small pores improved the water absorption of the matrix. The surface of the PP fibers was covered with mortar, which reduced the fluidity of the matrix, resulting in a decrease in the slump of the matrix. Similar results were reported by Akça et al. [59]: the matrix w/b ratio was 0.53, the RCA content was 25–55%; the consistency of the matrix was normal. Owing to the synergistic effect of the RCA and PP fibers, the consistence of the matrix was reduced.

Yazıcı et al. [60] examined the matrix slump when the steel fibers (SFs) (having 30, 60 and 60 mm long) aspect ratio (l/d) of hooked ends were 45, 46, and 80, and the SF contents in concrete were 0.5%, 1.0% and 1.5%. As the l/d ratio and $V_f$ of the SFs increased, the matrix slump decreased. This may be due to the network structure formed by the SFs in concrete and the large surface area of SFs, which increases the friction resistance inside the mixture and prevents the flow of concrete. Additionally, the slump of the RAC decreased as the SF content increased. When SFs (length is 30.5 mm and aspect ratio is 54.6) were present in the RAC, a cement paste was needed to cover them, which reduced the consistence of the mixture [61]. As shown in Figures 3 and 4, the slump of RAC is reduced by adding PP fibers or SFs to the matrix. As a result, some researchers have also added high-efficiency water reducers to the mixture to improve the consistence of RAC.

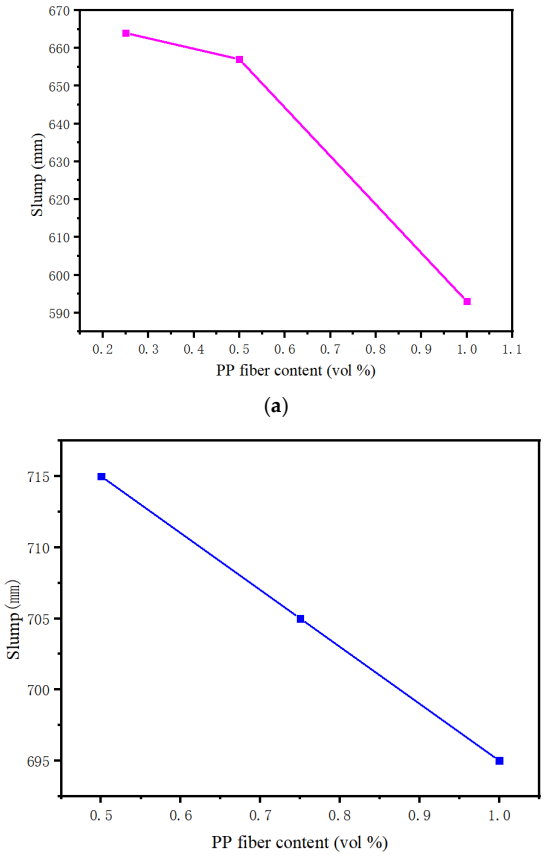
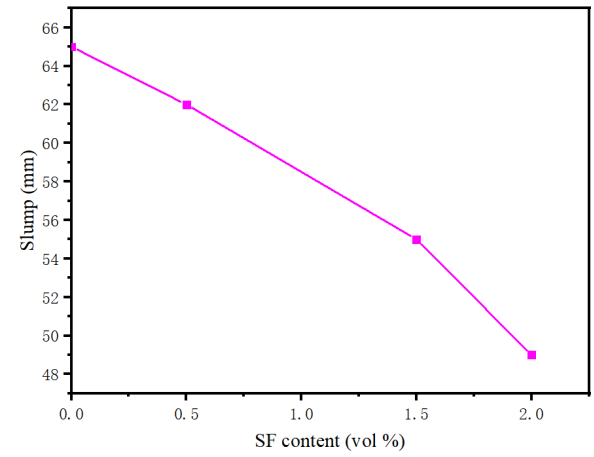
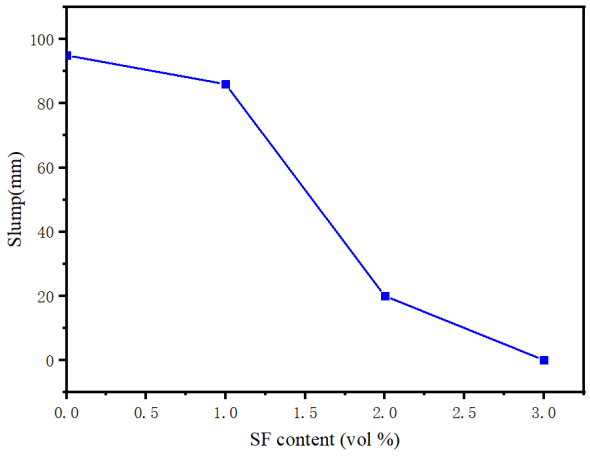



**Figure 3.** Effect of the PP fiber content on the RAC slump [58,62]. (**a**) w/b ratio of 0.5; (**b**) w/b ratio of 0.4.




(**a**)




(**b**)

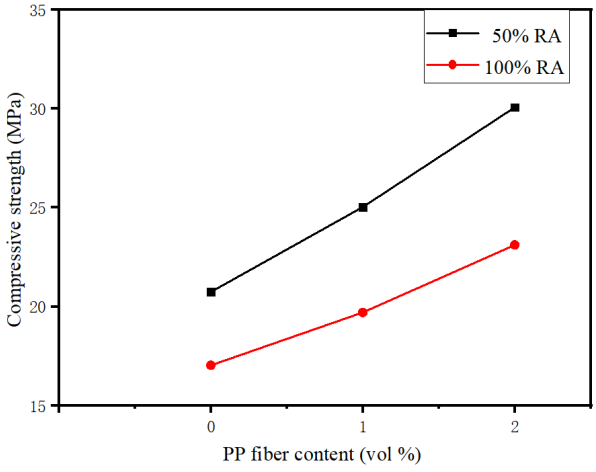
**Figure 4.** Effect of the steel fiber (SF) content on the RAC slump [63,64]. (**a**) w/c ratio of 0.39; (**b**) w/c ratio of 0.49.

## 3. Mechanical Properties of FRRAC

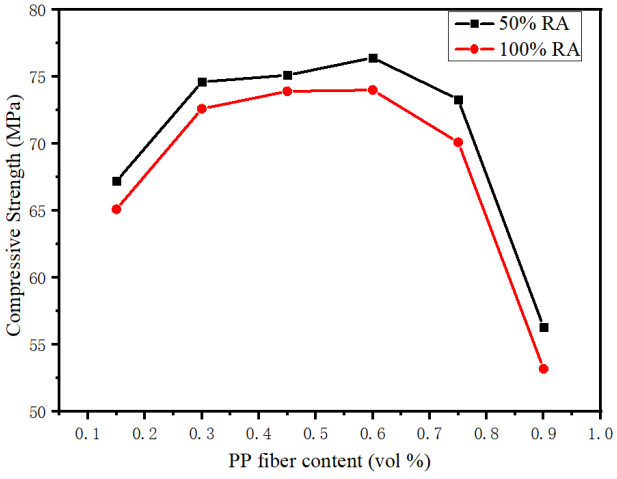
### *3.1. Compressive Strength*

As the PP fiber (length is 47 mm) content increases from 0 to 2%, the RAC compressive strength increases [65]. Zahid-Hossein et al. [66] reported that the compressive strength with 10% RCA in the matrix was superior to that with 30% RCA. This is similar to the results obtained by Choi and Yun [67] and may be due to the high water-absorption capacity of RCA compared with NA, which makes the internal hydration reaction of the substrate more complete. Adding 30% RCA increases the porosity of the concrete and reduces the compressive strength. The PP fibers act as bridges among the aggregate and the cement paste, delaying the crack propagation and improving the concrete strength.

As shown in Figure 5, the effect of RCA on the compressive strength of RCA is greater than that of PP fibers. Additionally, the optimal amount of PP fibers differs for different substrates. Therefore, the amount of RA added to concrete is ≤30%, and the appropriate amount of PP fiber added to the matrix can improve the compressive strength of the matrix. How to increase the replacement rate of NA with RA in concrete and keep the content of PP fiber (length is 12 mm) less than 0.6% to greatly improve the compressive strength of RAC is also a problem worth studying.




(**a**)




(**b**)

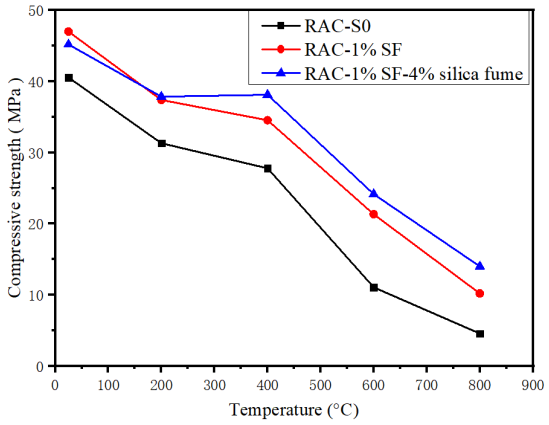
**Figure 5.** Effect of PP fibers on the compressive strength of RAC [65,68]. (**a**) w/c ratio of 0.55; (**b**) w/c ratio of 0.22–0.255.

With 0.7% SFs (length is 35 mm) added to the matrix, the matrix compressive strength is improved by approximately 10–19% [28]. The compressive strength with the addition of 1% SFs (length is 60 mm and aspect ratio is 65) to RAC was 3–14% higher than that of NAC. The shape and elastic modulus of the double-ended hook-shaped SFs can limit the propagation of cracks, increasing the RAC compressive strength [69]. The NA in the matrix is completely replaced with RA and is doped with 1% SFs (length is 13 mm). The FRRAC compressive strength is reduced by 5.85%, 20.4%, 20.3%, 27.9% and 38.0% at 25 °C, 200 °C, 400 °C, 600 °C and 800 °C, respectively. The optimal dosage of silica fume in the matrix is 4% [70]. The compressive strength and high temperature resistance of RAC can be enhanced by adding silica fume. The high $SiO_2$ content of silica fume produces a large amount of C-S-H gelling materials, ettringite (AFt) and AFm [71,72], which makes the matrix significantly dense and improves the density of the ITZ inside the matrix of RAC.

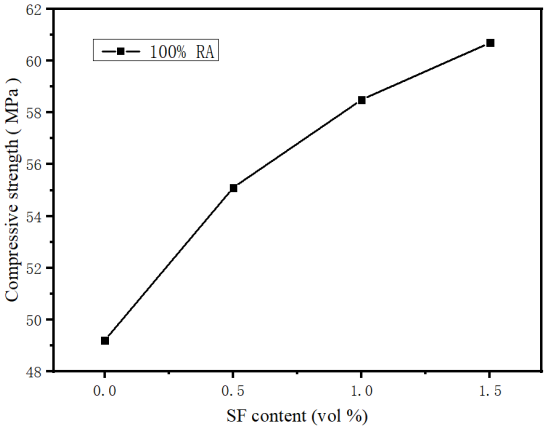
The FRRAC compressive strength decreases with the increasing temperature (Figure 6) [70]. The base body compressive strength does not decrease significantly in the range of 25–400 °C, but decreased greatly in the range of 400–600 °C. This is because the free water and adsorbed water in the matrix are evaporated from 25 °C to 200 °C. The resulting steam pressure destroys the microstructure of the concrete, reducing its compressive strength [73]. At 200–400 °C, the adsorbed water, interlayer water, and chemically bound water in the C-S-H gelling material are evaporated. The loss of moisture reduces the connection ability and the strength of the C-S-H cementitious material, reducing

the matrix compressive strength. Additionally, the slight disintegration of Ca $(OH)_2$ reduces the matrix compressive strength. The C-S-H gel already dehydrates from 100 °C, while calcium hydroxide dehydrates completely at 600–800 °C. Coarse aggregates (containing calcium carbonate) in the matrix also decompose, reducing the compressive strength of the matrix. Therefore, it can be concluded that FRRAC can withstand the high temperature of 400 °C, which reduces the compressive strength of the matrix very little.

The results obtained by Ahmadia et al. [74] indicated that the compressive strength effect of SFs (length is 30–70 mm) reinforced RAC was similar to that of SFs on NAC, or lower than that of NAC. The compressive strength of RAC mixed with an appropriate number of SFs was higher than that of ordinary concrete in the control group. Kachouh et al. [64] found that when the SF (length is 35 mm and aspect ratio is 65) content increased from 0% to 3%, the RAC compressive strength increased by 5.67–13.36%. When an appropriate number of SFs is added to the matrix, the number of plastic shrinkage cracks can be significantly reduced. Moreover, the three-dimensional disordered distribution of fibers and the high cohesive force of fibers with concrete make a strong network skeleton inside the concrete. According to the composite mechanical theory and the interface characteristics of SF–cement matrix, due to the existence of weak links in RAC, there are a large number of cracks, and the addition of steel fibers can cross both sides of the cracks, and the bonding characteristics of the interface are enhanced. The more fibers that cross the cracks in the unit area, the greater the crack resistance and reinforcement of the SFs. When SF content is high, SF distribution in the matrix is uneven, and the stress of the matrix will be concentrated, and the strength of the matrix decreases.




(**a**)




(**b**)

**Figure 6.** Compressive strength of RAC containing 1% SFs with different heating temperatures [70,75]. (**a**) w/c ratio of 0.46; (**b**) w/c ratio of 0.35.

Among the various combinations of hybrid fiber-reinforced composites in common concrete, SF and PP fibers are the most effective for improving the strength and ductility of the matrix. When both the SF (length is 50 mm and aspect ratio is 80) and PP fiber (length is 6 mm and aspect ratio is 300) contents were 0.5%, the compressive strength of SF–PP FRRAC is slightly higher than that of RAC with single-doped PP fiber, but slightly lower than that of RAC with single-doped SFs [62]. This is also similar to the research results of He et al. [75]. This may be related to the properties of the fibers [76]. The combination of SFs and PP fibers can enhance the mechanical properties of the matrix. PP fibers can pass through cracks, forming a fiber–cement base interface, and the interaction between the fiber and cement mortar can improve the performance of the matrix. Therefore, an appropriate number of SF (about 2%) and PP fibers (about 0.6%) was added into RAC with the content of RA less than 30%, which not only is able to improve the compressive strength of RAC but also reduce the cost of the concrete to the minimum [77,78].

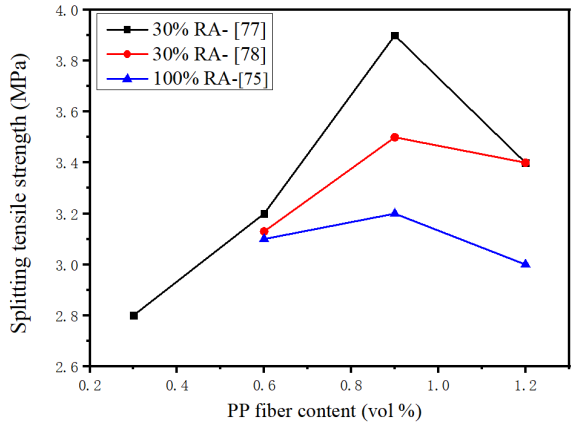
### *3.2. Tensile Strength*

The splitting tensile strength of FRRAC is related to the type of aggregate, the type of fiber, and the fiber volume content. Hanumesh et al. [65] performed numerous experiments using 25%, 50%, 75% and 100% RCA; 1% and 2% PP fibers (length is 47 mm) were used to manufacture the RAC. They found that when 1% and 2% PP fibers were added to the matrix containing 100% RA, the matrix splitting tensile strength increased by 34.84% and 85.6%, respectively, compared to the reference group. These results are consistent with those of Akça et al. [59], who reported that the splitting tensile strength of the matrix gradually decreased with an increase in the RA content. The addition of PP fibers can clearly enhance the splitting tensile strength of RAC.

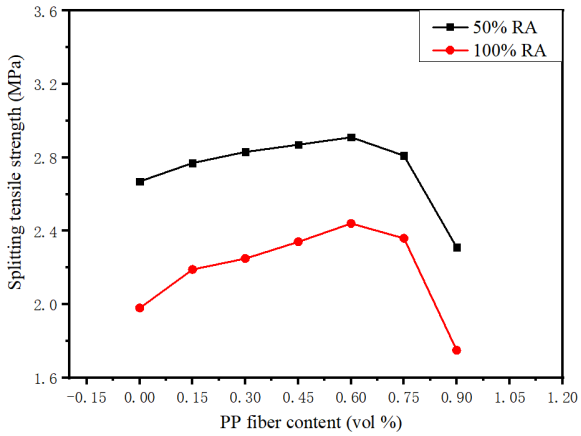
As shown in Figure 7a, the splitting tensile strength of the matrix first increased and then decreased with the increase in PP fiber content, and the optimal content of PP fiber was 0.9%. The elastic modulus of PP fiber is low, and the bonding slip characteristic of PP fiber and RAC determines the deformation performance of PP fiber after RAC cracking. When the matrix splitting failure occurs, PP fiber can be part of the load transfer to the fiber in the matrix; thus, the matrix can withstand a greater load, improving the cleavage strength of the substrate. As the PP fiber on the cracking surface is pulled out or the fiber on the cracking surface is gradually broken, the carrying capacity of RAC is gradually lost until the failure [79]. However, excessive PP fibers in the matrix will not distribute uniformly, which has adverse effect on tensile strength of RAC. Adding an appropriate amount of PP fibers to the matrix can improve splitting tensile strength. RAC splitting failure is mainly related to the interface between the RA and the newly added cement in the matrix, as well as the original interface of the RA.

Additionally, the water absorption of the RCA is enhanced when increasing the w/c ratio of the matrix. This increases the porosity of the matrix and reduces the bonding strength of the ITZs, reducing the matrix splitting tensile strength [80,81]. The addition of PP fibers can enhance the bonding of the ITZs, thus improving the splitting tensile strength of the matrix.

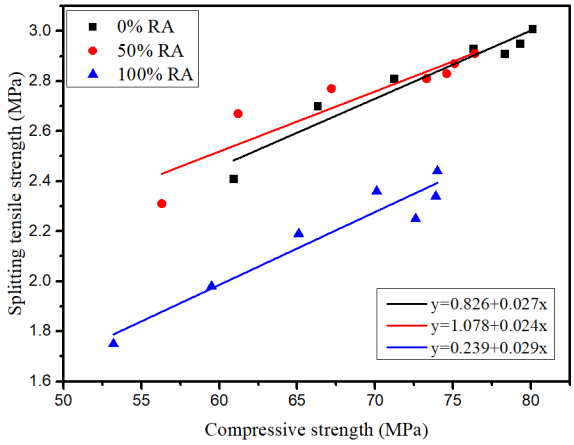
The splitting tensile strength of FRRAC is linearly related to its compressive strength. As shown in Figure 7, the splitting tensile strength increased with the compressive strength. When the content of PP fibers (length is 12 mm) varies from 0% to 0.9%, the compressive strength of the matrix is strongly correlated with the splitting tensile strength [68]. The effect of RA on the matrix splitting tensile strength was greater than that of the PP fibers. The addition of 30% RA improved the matrix splitting tensile performance, possibly because the surface of the RA was rough, the increase in the mechanical bite force between RA and the matrix, or the RA strength was high. The primary aggregate of the RA determines its strength. The splitting tensile strength of fine recycled aggregate (FRA) decreased by a smaller amount than that of the RCA did. This may be because there was more non-hydrated cement in the FRA; thus, a hydration reaction occurred, enhancing the matrix splitting tensile strength [82]. The optimal PP fiber content differs among different substrates. For different water–binder ratios, the optimal fiber content is different, but the optimal PP fiber content is generally between 0.6% and 1.5%.




(**a**) w/c ratio of 0.53




(**b**) w/c ratio of 0.22–0.255




(**c**) Relationship between the splitting tensile strength and compressive strength

**Figure 7.** Splitting tensile strength of RAC with different dosages of RA and PP fibers [59,68].

The splitting tensile test is relatively simple and feasible; thus, such tests have been widely performed [83]. Mohseni et al. [62] compared the effects of 0.5%, 0.75% and 1% SFs (length is 50 mm and aspect ratio is 80) on the RAC splitting tensile strength. They found that the splitting tensile strength was 44%, 66%, and 80% higher, respectively, than that without SFs. The splitting tensile strength was highest at 1% SFs. When both SF and PP fiber contents were 0.5%, the splitting tensile strength of the RAC enhanced by SF–PP fiber was slightly higher than that of RAC with single-doped PP fibers, but slightly lower than that of RAC with single-doped SFs. The SFs reinforced the concrete by acting as a bridge when the matrix was under tensile stress, inhibiting the formation and propagation

of cracks at the interface of the matrix. When the volume of SFs was too large, the concrete splitting tensile strength decreased.

In matrices with 50% and 100% RCA and 1% SFs (length is 60 mm and aspect ratio is 65), the splitting tensile strength with 30% GGBS was 7.18% and 3.44% higher, respectively, than that without GGBS [69]. This increase in the strength may have been due to the small particle size of the GGBS, which filled the pores of the RCA. GGBS can also improve the adhesion between the aggregate and the ITZs [84]. Therefore, adding GGBS to FRRAC can enhance the matrix properties. Additionally, the RCA performance affected the matrix splitting tensile strength. Using a high-strength RCA can increase the splitting tensile strength of the matrix, whereas using a low-strength RCA can reduce the splitting tensile strength of the substrate. High-strength RCA with new and old cement pastes has high interfacial bonding strength, and its rough surface can improve the microstructure of ITZs, which increases the splitting tensile strength of the matrix [85].

As shown in Figure 8, with the increasing of RA and SF contents, the matrix splitting tensile strength decreased and increased, respectively. For the SFs, exceeding the optimal dosage had a negative impact. Adding appropriate mineral additives and steel fibers to RAC can improve the splitting tensile strength of the matrix, but RA has greater impact on tensile strength than SF and mineral additives.

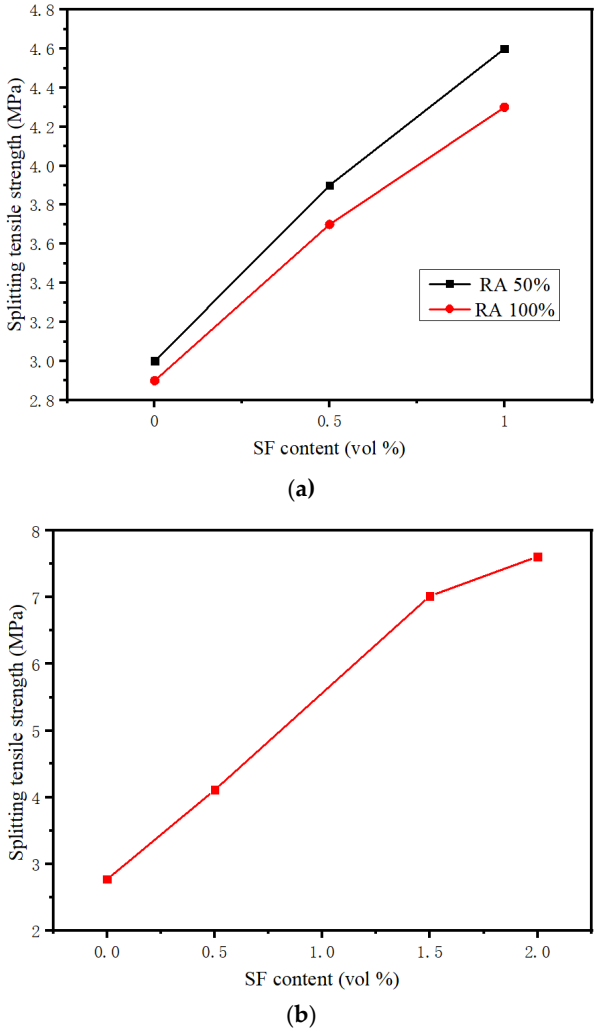



**Figure 8.** Effect of SFs on splitting tensile strength of RAC [61,74]. (**a**) w/c ratio of 0.54; (**b**) w/c ratio of 0.39.

According to the composite material theory and the concept of fiber constraint, the tensile strength expression of the matrix can be obtained as follows:

$$\sigma_t = \sigma_m[1 + \alpha\left(\frac{l}{d}\right)V_f] \quad (5)$$

where $\sigma_m$ is the tensile strength of fiber-reinforced concrete, $V_f$ is the volume ratio of fibers, $\frac{l}{d}$ is the length–diameter ratio of the fibers, $\alpha$ is the comprehensive influence coefficient of fiber resistance to flexural strength.

Therefore, it can be seen from Equation (5) that the greater the content of PP fiber and SFs in a certain range, the greater the tensile strength of the matrix under the same other conditions.

### *3.3. Flexural Strength*

The flexural strength is an important strength index of concrete. The flexural strength of the aggregate and the cement mortar significantly affects the concrete flexural strength [86]. However, RAC contains impurities, such as brick, glass, and wastepaper, which weaken the bond between the RAC and the cement mortar, reducing the RAC flexural strength [87]. Researchers have added PP fibers and SFs to the RAC to enhance the RAC flexural strength.

Ahmed et al. [68] examined the effect of the PP fibers (length is 12 mm) content on the flexural strength of RAC and revealed the relationship between the compressive strength and flexural strength of RAC with different RA contents. The results are presented in Figure 9. When the PP fiber content increased from 0 to 0.6%, the RAC bending strength increased. When the PP fiber content increased from 0.6% to 0.9%, the RAC bending strength decreased. The substrate compressive strength had a good relevance with the flexural tensile strength. However, according to the results of a variance analysis, the aggregate type has a greater influence on the flexural strength of concrete than the PP fiber content. A larger peak pull load corresponded to a stronger bond between the matrix and the PP fibers (length is 50 mm) [59]. Zahid-Hossein et al. [66] investigated concrete containing 30% RCA and found that the flexural strength of the matrix with 2% PP fibers (length is 12 mm) was 6.13% higher than that without PP fibers. This may have been due to the enhancement of the fiber–matrix bond. The optimal PP fiber content differs among different matrices. Therefore, adding an appropriate amount of PP fiber into the matrix can improve the bending strength of the matrix.

As shown in Figure 10, the first-peak strength ($f_1$), peak strength ($f_p$), and equivalent initial flexural strength ($f_{e,p}$) of RAC were correlated with the flexural strength. When SF content was <0.5 vol%, the RAC flexural strength did not increase significantly. When the volume content of SFs was 0.5–2%, the flexural tensile strength of the RAC gradually increased. When the SF content is enhanced from 0 to 1.5%, the flexural tensile strength of RAC is enhanced by 33.3% [75]. The SFs enhanced the matrix after cracking, which is similar to their effect on NAC [88].

Carnerio et al. [28] reported that the inclusion of 0.75% hooked-end SFs (length is 35 mm) enhanced the substrate flexural tensile properties by 36%. Yoo et al. [89] concluded that the flexural strength of high-strength concrete increases significantly when the hooked-end SFs (length is 13 mm and aspect ratio is 65) content is ≥1%. However, double-hook-end SFs (length is 60 mm) have a better strengthening effect than single-hook-end SFs (length is 60 mm), possibly because a specimen containing double-hook-end SFs needs a larger drawing force when it fails [90]. As the surface of RCA is rough, it bonds well with the fiber and produces an interlocking effect, increasing the bending strength of the matrix. The addition of GGBS to FFRAC can also improve the bending tensile strength of the matrix, possibly owing to the increase in the bending tensile strength of the matrix due to the filling effect of GGBS and the volcanic-ash effect [69]. The optimal SF dosage is generally about 1–3%. Therefore, mineral materials and fibers can be added to increase the tensile strength of the matrix.

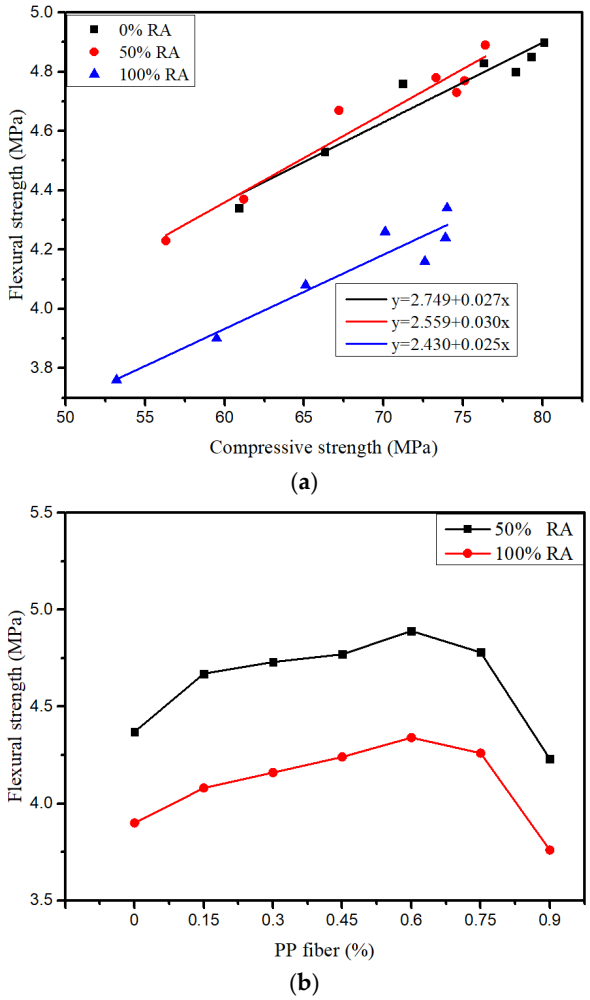



**Figure 9.** Flexural strength of RAC with different RA contents [68]. (**a**) Relationship between the flexural and compressive strength; (**b**) Effect of the PP fiber content (%).

According to the composite theory, the flexural strength of concrete can be calculated as follows:

$$f_{ftm} = f_{tm}(1 + \alpha_{tm}\, \rho_f\, l_f) \quad (6)$$

where $f_{ftm}$ is the flexural strength of concrete (MPa), $f_{tm}$ is the flexural strength of matrix concrete (MPa), $\rho_f$ is the volume ratio (%) of fiber, $l_f$ is the length of SF (mm), $\alpha_{tm}$ is the comprehensive influence coefficient of fiber against flexural strength.

From Equation (6), it can also be seen that the flexural strength of FFRAC gradually increases with the increase in fiber content.

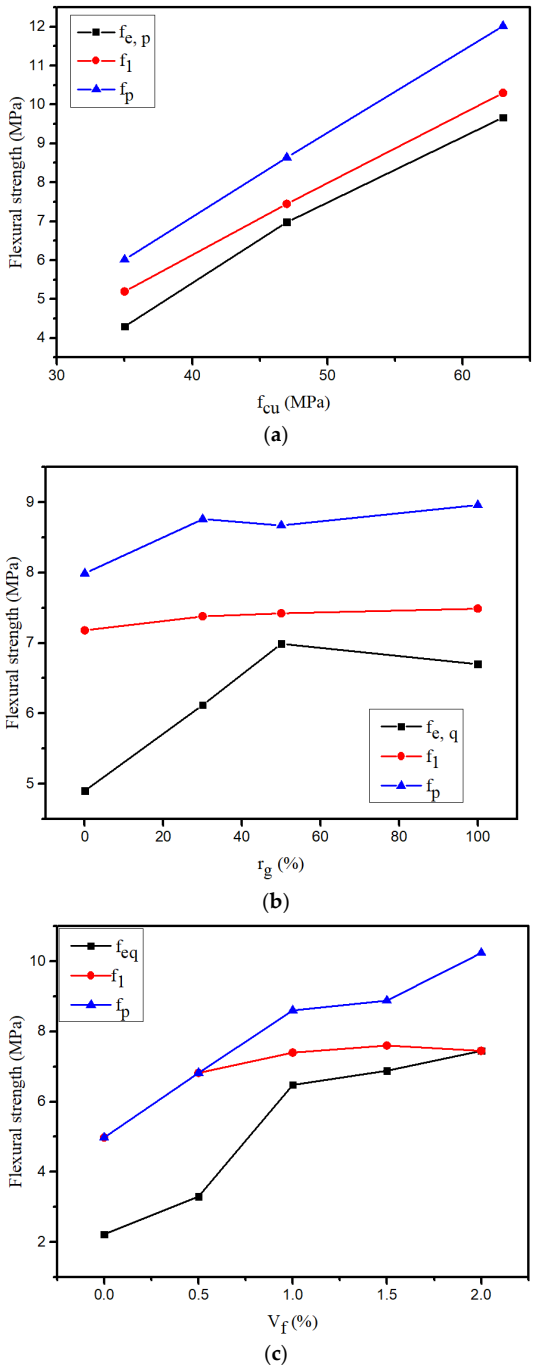



**Figure 10.** Effects of different compressive strength, RA contents, and SF contents on the flexural strength [61]. (**a**) Compressive strength (MPa); (**b**) RCA content (%); (**c**) SF volume fraction (%).

### *3.4. Stress–Strain Relationship*

Previous studies have indicated that PP fibers significantly affect the stress–strain curve of RAC. As shown in Figure 11, when the PP fiber content ranged from 0.5% to 1%, the peak stress and strain of the specimen decreased. The stress–strain property of the matrix can be improved by adding appropriate amount of PP fibers. This is mainly because PP fibers (length is 12 mm) can act as a bridge to prevent cracks from growing, thereby reducing the strain [79]. The peak strain of the RAC was higher except for the sample with 1% PP content. This is because the RA aggregate was loose and porous, which lead to premature cracking of the matrix.

The RAC stress–strain curve is generally separated into the following four stages: (1) Elastic stage: Although there are holes and microcracks inside the specimen, the external load on the specimen is small, and the cracks inside the specimen do not propagate. The addition of fibers can prevent the growth of microcracks. (2) Elastic-plastic stage: With an increase in the external load, the cracks expand, even if the fibers only prevent the cracks from expanding. (3) Yield stage: The cracks continue to expand, and there is critical stress propagation. (4) Fracture stage: The cracks expand stably and reach the critical length. During the stress–strain process of NAC, the cracks spread through the cement paste, whereas the strength and stiffness of the RA in RAC were low, and the cracks spread through the aggregate.

The factor influencing the RAC crack cracking is the deformation of transition zone. The RA surface is rough and porous, which is closer to the stiffness and elasticity of the surrounding mortar and has better bonding performance, improving the strength of the ITZ [28] and reducing the cracking of the matrix. Similar behavior was observed in another study [91]. The fibers in FRRAC can bond with ITZ more effectively, improving the stress–strain behavior of the matrix.

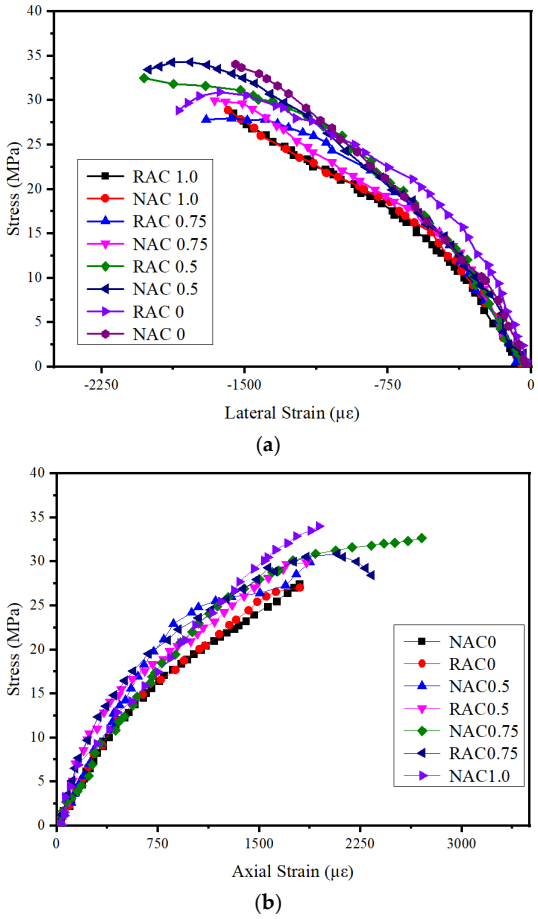



**Figure 11.** The stress–strain curves with different PP fiber contents [79]. (**a**) Lateral strain; (**b**) Axial strain.

Figure 12a–c present the stress–strain curves of the RAC with different contents of SFs, RAC and silica fume, respectively. As shown in Figure 12a, the SF content significantly affected the peak strain of the matrix. With the addition of 1%, 2%, and 3% SFs to the matrix, the peak strain of the matrix was enhanced by 160%, 197%, and 234% compared to the peak strain without SFs. For concrete with RCA contents of 30%, 70%, and 100%, the addition of 1% SFs increased the peak strain by 98%, 46% and 35%, respectively. Therefore, the concrete containing RCA was mixed with an appropriate number of SFs to improve the deformation resistance of the matrix. SFs can bridge with RAC in the matrix, resist the deformation of the matrix, and enhance the deformation capacity of the RAC. With the addition

of SFs, the RAC toughness was improved, as indicated by the lope of the declining branch of the stress–strain curve. The compression performance of the matrix was similar to that of fiber-reinforced NAC [28].

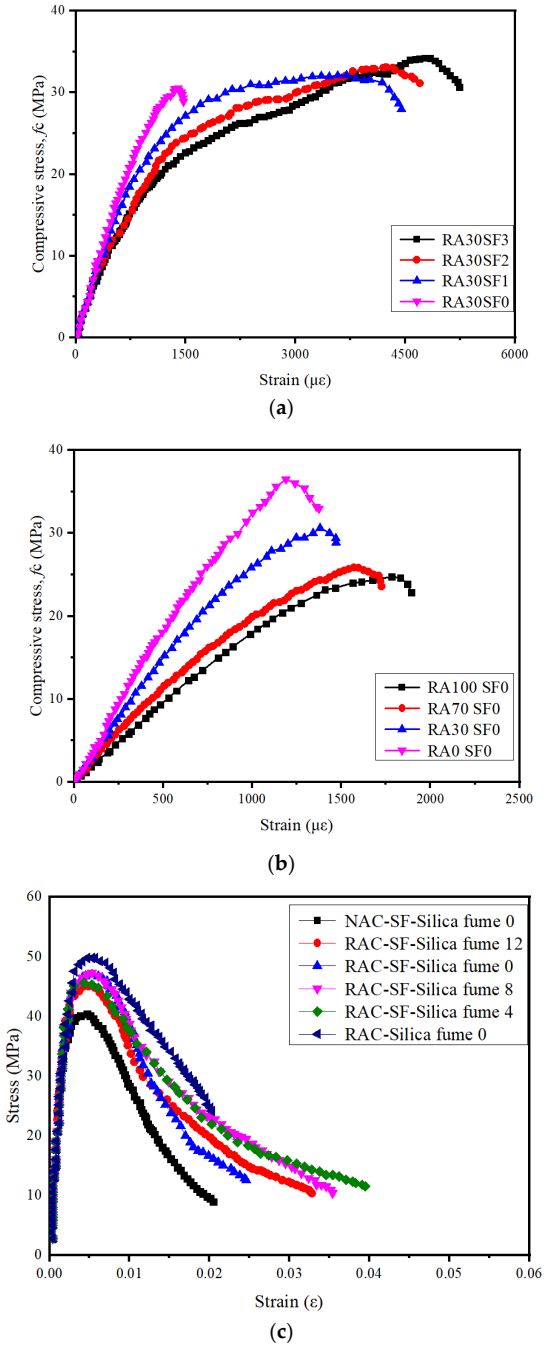



**Figure 12.** Stress–strain curves of RAC [64,70]. (**a**) Effect of the SF content (%); (**b**) Effect of the RA content (%); (**c**) Effect of the silica fume content (%).

With an increase in the SF content, the crack volume in the matrix increased, and the critical stress–strain value decreased. Owing to their high transverse strain capacity, SFs can not only transfer energy in the matrix, but also bridge cracks. SFs enhance the energy absorption capacity of the concrete, improving the stress–strain capacity of the matrix. They can prevent crack propagation, and fiber bridge crack behavior can improve the post-peak ductility. As the fiber is strengthened, the slope of the stress–strain curve decreases [92–94].

However, an excessive SF content negatively affects the stress–strain curve of the matrix. As shown in Figure 12b, the slope of the stress–strain curve for the RAC increased with the decreasing RCA dosage. This was mainly due to the low density and elastic modulus of the RCA, which resulted in a low density and elastic modulus of the matrix [64]. As shown in Figure 12c, adding 4% silica fume to the matrix improved the stress–strain curve of the matrix. In the study of Xie et al. [70], the slope of RAC in the upper and lower parts of the stress–strain curve gradually flattened when the temperature ranged from 25 °C to 800 °C, and RAC peak stress and Young's modulus decreased at high temperatures. The base bearing loading capacity and stiffness were reduced mainly because the RA contained more pores and could absorb more water than NA. At high temperature, the moisture of the matrix evaporates, increasing the number of pores in the matrix. When SFs were added to the matrix, their thermal-conductivity effect caused the interior of the matrix to be uniformly heated at high temperatures; thus, the stiffness and peak strain of the matrix were higher than those of the matrix without SFs. The stress–strain effect of RAC with SF content of about 3% was better.

### *3.5. Elastic Modulus*

According to the standard definition used in China, the elastic modulus is the slope value of the stress–strain curve of the specimen 1/3 away from the peak load (GB50081-2002) [95]. The matrix elastic modulus is the ratio of the specific limit stress of the concrete material to the corresponding strain. Therefore, a higher elastic modulus of the concrete admixture corresponds to a higher strength of the substrate. The old mortar and impurities attached to the RA reduce the matrix elastic modulus. When the NA in the matrix is completely replaced with the RA, the concrete-specimen elastic modulus was reduced by 45% and 48% in the studies of Xiao et al. [19] and Xie et al. [96], respectively. Sato et al. [97] reported that when the proportion of RA replacing NA was 100%, the concrete Young's modulus was reduced by 15% compared with the reference group. Owing to the high contents of old mortar and impurities in the RA, the number of interfaces in cement mortar was large. Additionally, at the interface, there were numerous microcracks, and the porosity was high, giving the RAC a high deformation capacity under an external load [98].

RA is more easily deformed than NA due to its own characteristics, and the poor interfacial adhesion between the aggregate and the old slurry results in more capillary pores and microcracks on ITZ. Therefore, the total replacement of NA by RA will have a negative impact on the matrix stiffness. The difference of concrete elastic modulus ratio is mainly caused by the difference of aggregate properties and the difference of reference formula. Some scholars have studied the elastic modulus of recycled aggregate concrete mixed with PP fiber or SF.

As shown in Figure 13, when the volume content of PP fibers increases gradually, the elastic modulus of the matrix decreased. Ahmed et al. [68] reported that when the PP fiber (length is 12 mm) content increased from 0 to 0.6%, the elastic modulus of the matrix increased. When the PP fiber increased from 0.6% to 0.9%, the elastic modulus decreased. After the addition of 0.9% PP fibers to the RAC, the matrix elastic modulus was reduced by 3.38% compared to that without PP fibers. The combined effects of RA and PP fibers led to the reduction in the RAC elastic modulus. There were many PP fibers in the matrix, and they were unevenly distributed, and easy to cause agglomeration, leading to cracks in the matrix. Therefore, the elastic modulus of the matrix was reduced. The elastic modulus of matrix can be improved by adding PP fibers (about 0.6%) to RAC.

When 1%, 2%, and 3% SFs were added to RAC, the elastic modulus of the RAC increased by 8%, 11%, and 17%, respectively [64]. By adding an appropriate number of SFs, the compressive strength of the matrix was improved, along with the elastic modulus. Among all the mechanical properties, the temperature has the greatest influence on the elastic modulus of the matrix [99]. Xie et al. [70] reported that at 25 °C, 200 °C, 400 °C, 600 °C and 800 °C, the elastic modulus of SF reinforced RAC (SFRAC) was 3.7%, 2.7%, 32.5%, 123.6%, and 89.7% higher, respectively, than that of RAC. The bridging, stretching, and deformation resistance of the SFs in the high-temperature environment of the matrix were investigated [100]. The matrix elastic modulus decreases with the increasing of RA content

and temperature. Most research results indicate that the concrete elastic modulus increases with the SF content.

As shown in Figure 14, with the increase in SF content, the matrix elastic modulus decreases, which may be related to the type and performance of SFs. The concrete compressive performance is linearly dependent on the elastic modulus. However, an appropriate number of SFs can also increase the elastic modulus of RAC, and the increase in temperature and RA content can reduce the elastic modulus of the matrix. Considering the influence of SF content on RAC cost, adding about 3% SF into the matrix can greatly improve the elastic modulus of the matrix.

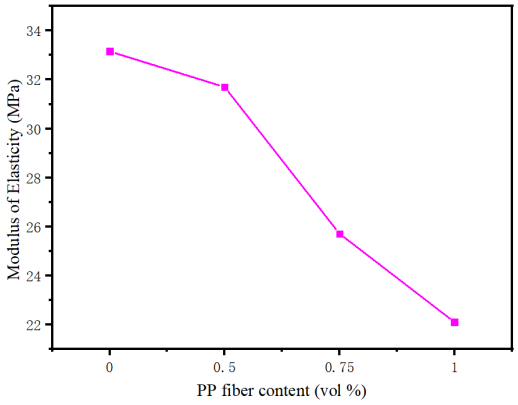
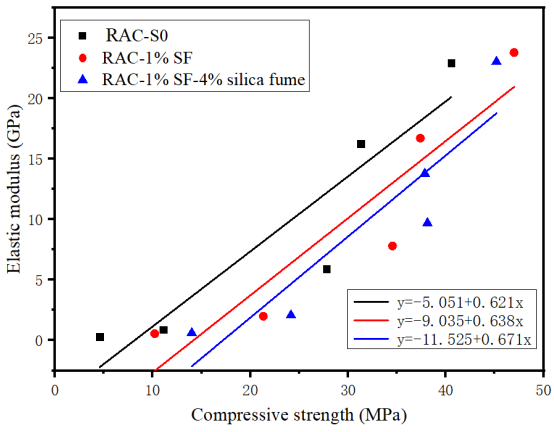
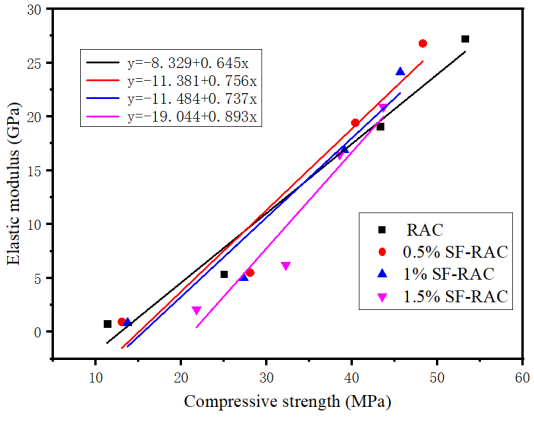



**Figure 13.** Effects of PP fiber content on the elastic modulus [76].




(**a**)




(**b**)

**Figure 14.** Relationship between the compressive strength and the elastic modulus [70,101]. (**a**) w/c ratio of 0.46; (**b**) w/c ratio of 0.48.

## 4. Durability of FRRAC

### *4.1. Chloride ion Permeability*

Chloride-ion penetration is an important index of concrete durability, as chloride often causes corrosion of reinforced concrete and reduces the service life of the concrete. Adding inhibitors to concrete can slow the corrosion due to chloride ions. The addition of silica fume to concrete results in pozzolanic reaction to produce C-S-H, and the aggregate effect and filling effect of silica fume can improve the compactness of the matrix and inhibit the corrosion and penetration by chloride ion [102,103]. The chloride-ion permeability of the test piece increased with the PP fiber and SF contents (Figure 15). The permeability of chloride ions was measured via a rapid chloride permeability test. Chlorine ions also corrode SFs in the matrix. There was certainly error in the test, because SFs have conductivity.

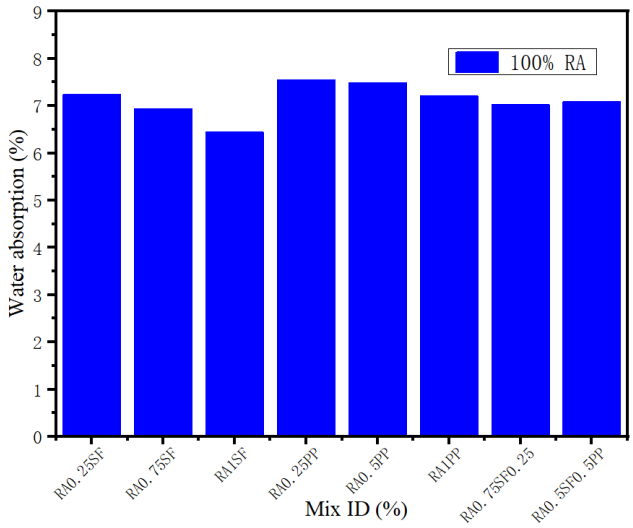



**Figure 15.** Effect of fibers in RAC on the charge passed [62].

The chloride permeability of the matrix increased with the RA content (Figure 16). This is because there were more ITZ species in RAC than in the NAC, and there were more microscopic cracks in the ITZs. There were many pores in the RA, which connected the microscopic pores in the matrix and provided channels for chloride-ion penetration. With the increasing SF content, the matrix chloride permeability decreased (Figure 16). The addition of SFs enhanced the compactness of the matrix. When RHA was incorporated, it had pozzolanic and filling effects and improved the density of the matrix. SFs and RHA can play a synergistic role in reducing the chloride permeability of the matrix. Additionally, when SF was added to the specimen, the calcium hydroxide solution reacted with the SFs. Therefore, the standard wet–dry cycle method can be used to determine the chloride penetration capacity of specimens.

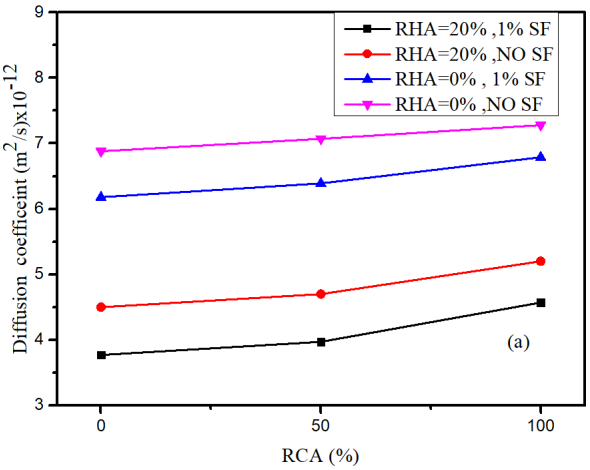



**Figure 16.** Effect of the RCA content of RAC content on the charge passed [41,62].

### *4.2. Carbonation Resistance*

Carbonization of concrete refers to the chemical reaction between carbon dioxide in the air and calcium hydroxide, as shown in Equations (7)–(10), to produce calcium carbonate and water. Carbonation causes concrete shrinkage (carbonation shrinkage), which can easily lead to cracks on the concrete surface. The carbonation depth of the matrix increases with the carbonation reaction time [6]. The porosity and permeability of RAs are higher than those of NAs, which encourages the entry of $CO_2$. Therefore, the carbonation rate of RCA is faster than that of NAC. $CaCO_3$ produced by carbonation of RCA will make the matrix compact and have some favorable effects on the matrix.

$$CO_2 + H_2O \rightarrow H_2CO_3 \quad (7)$$

$$Ca(OH)_2 + H_2CO_3 \rightarrow CaCO_3 + 2H_2O \quad (8)$$

$$3CaO{\cdot}SiO_2{\cdot}3H_2O + 3H_2CO_3 \rightarrow 3CaCO_3 + 3SiO_2 + 6H_2O \quad (9)$$

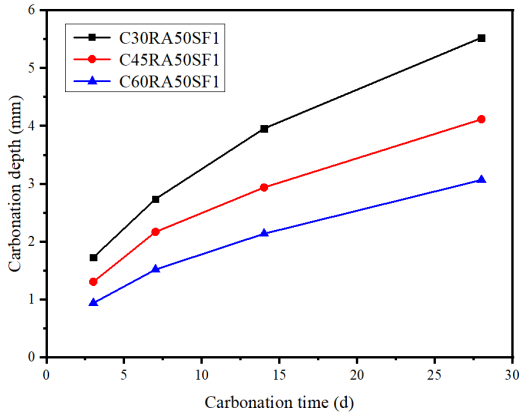
$$2CaO{\cdot}SiO_2{\cdot}4H_2O + 2H_2CO_3 \rightarrow 2CaCO_3 + 2SiO_2 + 6H_2O \quad (10)$$

As the number of cycles undergone by the RA increases, the amount of mortar that is combined with RA gradually increases, increasing the porosity. Therefore, the RAC carbonation resistance decreases. Over time, the carbonation rate of concrete decreases [104]. While RCA contains old mortar, which makes the amount of cement in RAC larger than NAC, and the carbonated materials in the matrix increase, thus improving the carbonation resistance of the matrix. However, dry RA has higher water absorption, which can reduce the w/c ratio and porosity of the matrix and improve the carbonation resistance of the matrix [105].

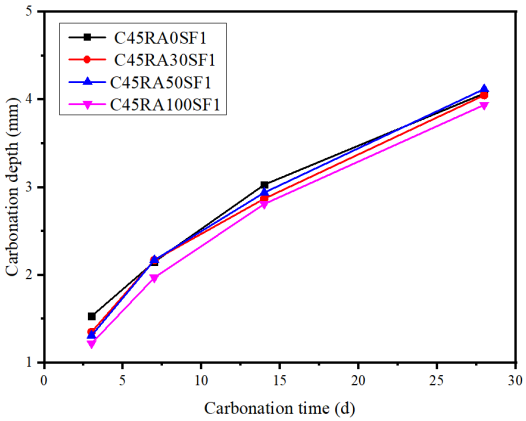
When the content of RCA is less than 25%, the resistance to carbonation of the matrix is similar to that of NAC [106,107]. The carbonation resistance of RAC containing PP fibers is not affected by the amount of PP fibers. Calcium carbonate and other chemical substances produced by carbonation of the matrix can fill the pores of the matrix and make the matrix denser, which not only reduces the porosity and water absorption capacity of the matrix but also improves the RAC compressive strength [108]. When the w/c ratio of concrete is within an appropriate range, the carbonation rate increases with the w/c ratio, and the carbonation depth decreases with the increasing matrix compressive strength [109,110].

As can be seen from Figure 17, when the SFs' (length of 30.5 mm, and aspect ratio of 54.6) volume content is between 0 and 1.5%, the carbonation depth of RCA at each age gradually decreases. This is because adding an appropriate number of SFs into the matrix can improve the compactness of the matrix, make it difficult for $CO_2$ to enter the matrix and slow down the carbonation rate. When the SF content increases from 1.5% to 2%, due to the uneven distribution of the excess SFs in the matrix, the

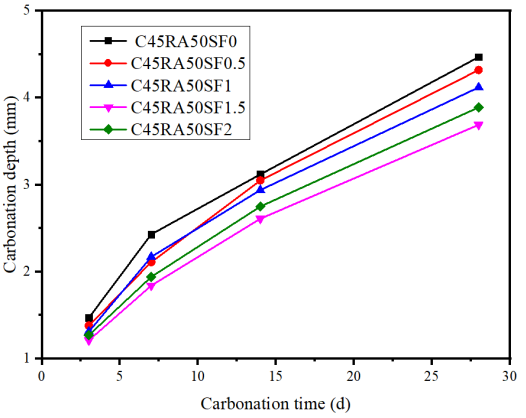
bond strength between SFs and the matrix decreases, and the compaction degree of concrete decreases, so the carbonation depth increases [63]. The greater the strength of matrix, the greater the compactness of matrix. Carbon dioxide in the air is more difficult to enter into the matrix for carbonation reaction. Carbonation of matrix will reduce the content of carbon dioxide in the air. Carbonation reduces the pH of the matrix. This will lead to the deterioration of the SF surface protective film and even lead to the corrosion of SF, thus reducing the performance of the matrix. PP fiber has acid resistance and alkali resistance; the decrease in pH value has no great influence on the matrix containing PP fiber.




(**a**) Matrix strength grade (MPa)




(**b**) RCA content (%)




(**c**) SF content (%)

**Figure 17.** Carbonation depth with different carbonation time [63]. (**a**) Matrix strength grade (MPa); (**b**) RCA content (%); (**c**) SF content (%).

### *4.3. Freezing–Thawing Resistance*

RAs have a higher water absorption capacity than NAs; a high moisture content in the matrix pores is unfavorable to the freeze–thaw resistance of concrete [111]. After 300 freeze–thaw cycles, the matrix mass loss improves with the growth of w/b ratio (0.43, 0.48 and 0.53) and RA content of matrix, and also enhances with the growth of cycle times [112]. Increasing the RA content increased the number of cracks in the matrix, which increased the mass loss of the matrix. The RA had a higher water absorption capacity than the NA did, which negatively affected the anti-freeze–thaw performance of the matrix. However, when 5% of the air entraining agent was added to RAC, its durability became comparable to that without an air entraining agent NAC. As shown in Figure 18, after 56 freeze–thaw cycles, the NAC compressive strength was reduced by approximately 70%, the RAC compressive strength was reduced by 24%, and the compressive strength of RAC containing PP fibers with entraining air was reduced by 7% [113]. Therefore, adding a large amount of RA to RAC will reduce the freezing–thawing resistance of the matrix, while adding an appropriate amount of PP fiber can improve the freezing–thawing resistance of the matrix.

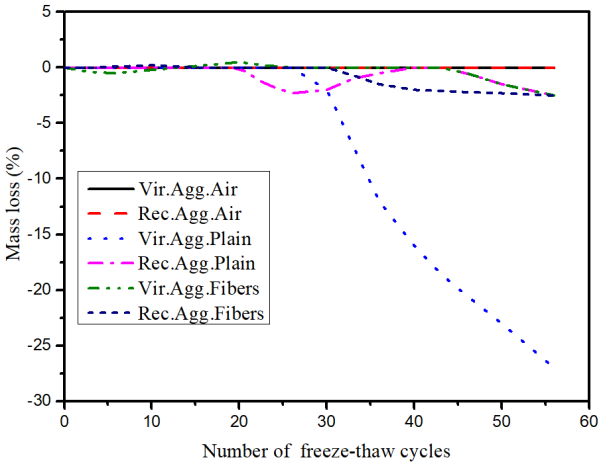



**Figure 18.** Mass loss of PP fiber reinforced RAC after freeze–thaw cycling [113].

After 50 freeze–thaw cycles, the RAC tensile strength was reduced by only 10% compared with the initial value. During the freeze–thaw cycles, PP fibers (length is 54 mm) have an interlock effect, while RA can be freeze-cracked, thus reducing the tensile strength of matrix [114]. Gao et al. [63] examined the freeze–thaw cycling behavior of the matrix when the concrete compressive strength was 60 MPa, the replacement rate of RA was 50%, and the SF content was 1%. They found that after 300 freeze–thaw cycles, the mass loss rate was just 0.2%.

Among the parameters studied, the number of freeze–thaw cycles had the greatest impact on the concrete mass loss rate. The mass loss increased or decreased with the freeze–thaw cycling, which may have been related to the SFs, RA and mortar interaction. With the increase in freeze–thaw cycles, more cracks appear in the matrix, which makes the matrix absorb more water. This water can corrode SFs, and the weight of corroded SFs increases, which also leads to the improvement of matrix weight. With the increasing of SF content, the mass loss of RAC first increased and then decreased, and, additionally, the mass loss decreased with an increase in the matrix strength (Figure 19).

Adding PP fiber and SF to RAC can improve the freezing–thawing resistance of RAC because the fibers in the formation of the three-dimensional grid in RAC can inhibit the formation and development of early shrinkage cracks and segregation cracks in RAC, which improves the ability of the matrix to resist freezing–thawing. The excellent bonding performance between the fibers and RAC matrix can also prevent the overflow of bubbles during the preparing process of RAC mixture. With the increase in gas content in RAC, the fiber can relieve the expansion stress during the freeze–thaw cycle and the freeze–thaw resistance of the matrix can be improved.

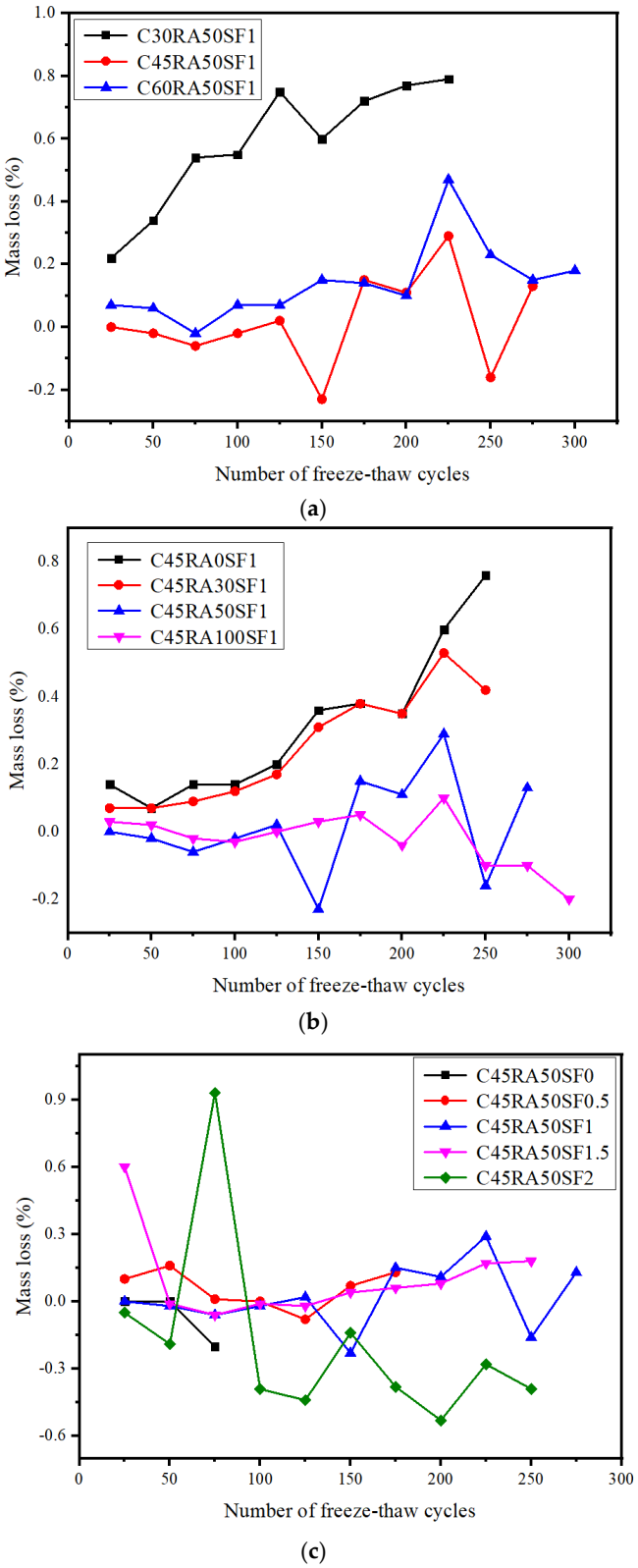



**Figure 19.** Mass loss of RAC reinforced with SFs after freeze–thaw cycling [63]. (**a**) With different matrix strength grades (MPa); (**b**) With different RA contents (%); (**c**) With different SF contents (%).

### *4.4. Shrinkage Performance*

The shrinkage of concrete refers to the phenomenon of volume reduction in the initial stage of concrete setting or in the process of concrete hardening. The shrinkage is generally divided into

plastic shrinkage (also known as shrinkage), chemical shrinkage (also known as self-shrinkage), drying shrinkage, and carbonation shrinkage. A large degree of shrinkage can cause concrete cracking. Drying shrinkage refers to the shrinkage of concrete due to moisture evaporation. Mainly because of the moisture from C-S-H transported into the pores, and then evaporated from the pores, was the volume shrinkage of the matrix caused. When the RA content increased from 0 to 100%, the drying shrinkage rate of concrete gradually increased [115]. In a matrix containing 100% RA, the drying shrinkage rate of the RAC after 180 d was 70% higher than that of a reference group [116]. The use of RA increases the amount of cement paste (both old and new) in the matrix. There are many microcracks in the old cement mortar, increasing the porosity of the concrete. Moreover, owing to its high porosity, the RA can absorb much water; thus, much evaporated water is present in the matrix, and this leads to the drying shrinkage of the RAC [117].

As shown in Figure 20, when the PP fiber (length is 10 mm) content was 0.25%, the matrix shrinkage was reduced by approximately 6% [118]. This may be because the fibers prevented the cracks from spreading in the matrix. With the increasing PP fiber content, the shrinkage of the matrix increased. This may have been due to the increased content of PP fibers and their uneven distribution in the matrix. Over time, the matrix free shrinkage gradually improved. From Figure 21, it can be seen that the shrinkage strain of RAC reinforced with double-hook-end SFs (length is 60 mm and aspect ratio is 65) was lower than that of RAC reinforced without double-hook-end SFs. At 400 d, under the conditions of 1% SFs and 100% RCA, the free shrinkage of R80 and R40 (RCA is derived from parent concrete with compressive strength of 80 MPa and 40 MPa, respectively, and is called R80 and R40) matrix was reduced by 6.25% and 13.04%, respectively, compared with those without SFs. The reduction in the shrinkage strain was mainly due to the bridging action of SFs to prevent the expansion of shrinkage strain cracks in concrete, which is consistent with the previous research results [119,120]. The shrinkage strain decreases with the increase in matrix strength. The addition of an appropriate amount of fiber in RAC can reduce the shrinkage of matrix, but the cost factor also should be taken into account, which will affect the promotion and use of FRRAC.

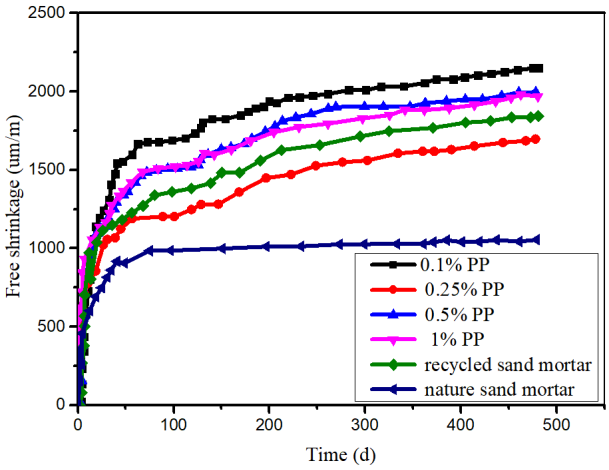
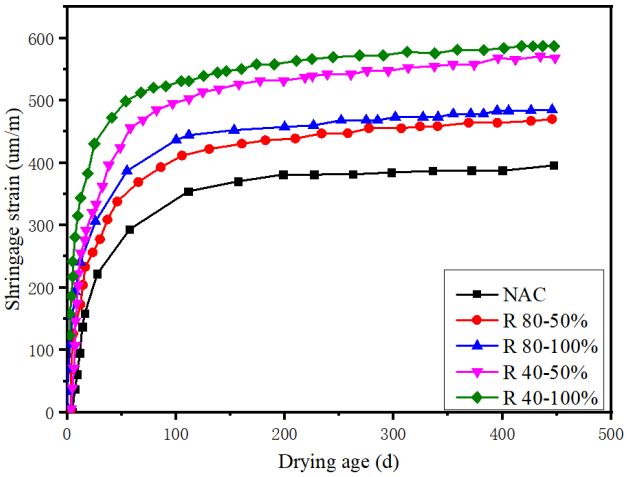
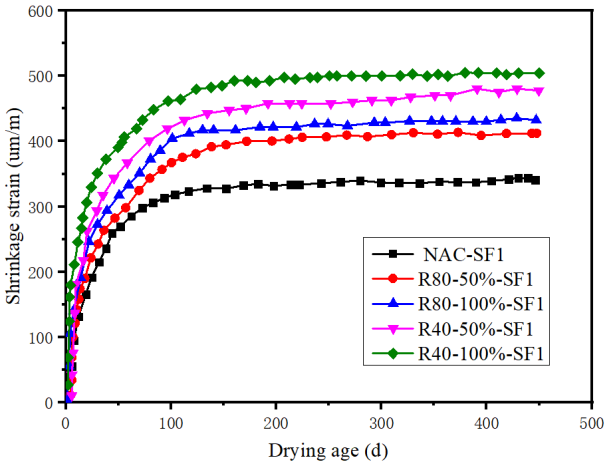



**Figure 20.** Effect of PP fibers on the free shrinkage [118].




(**a**) Without SFs

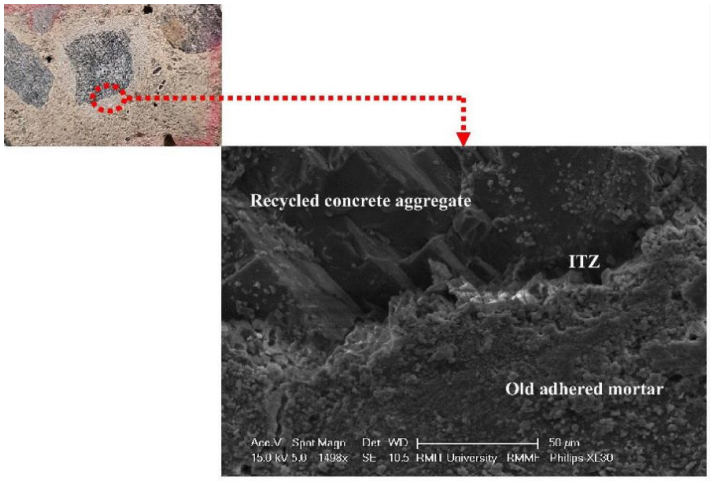



(**b**) Reinforced with SFs

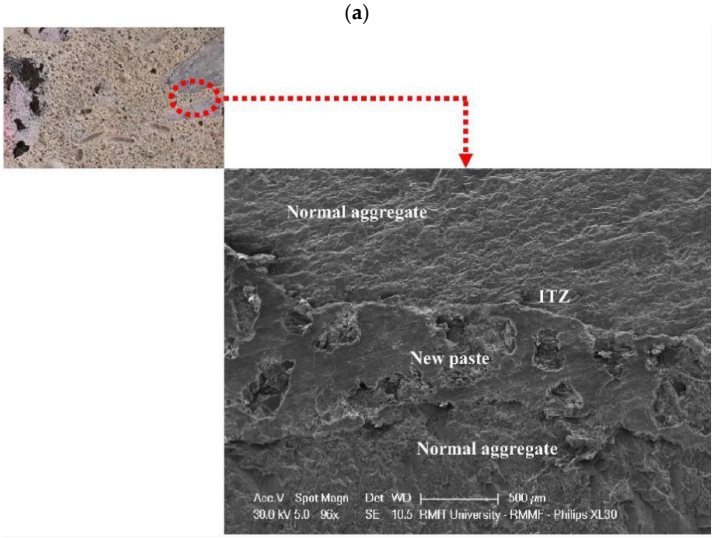
**Figure 21.** Shrinkage strain of RAC with respect to the drying age [69]. (**a**) Without SFs; (**b**) Reinforced with SFs.

## 5. Microstructure of FRRAC

Poon et al. [26] found that there were loose and porous water particles in the ITZs of ordinary RAC. The hydrates in the ITZs of traditional concrete and high-performance RAC were relatively dense, and the hydrates in the ITZs significantly affected the mechanical properties of the concrete. Figure 22 presents microstructure analysis results for RAC and NAC. Figure 23 shows that there are many pores and cracks in the mortar around RCA, which is the same as the research results of Afroughsabet et al. [69]. This led to the high water-absorption capacity of the RCA. The adhesion among the aggregates in the NAC and the cement mortar was good, and the interface was relatively dense and without cracks [121]. The ITZ of the RCA was relatively weak, and the interface was prone to cracking, mainly because of the high porosity of the old mortar and the easy absorption of water, resulting in a low w/c ratio. The interface could not produce compact hydration products, such as C-S-H crystals and calcium hydroxide.

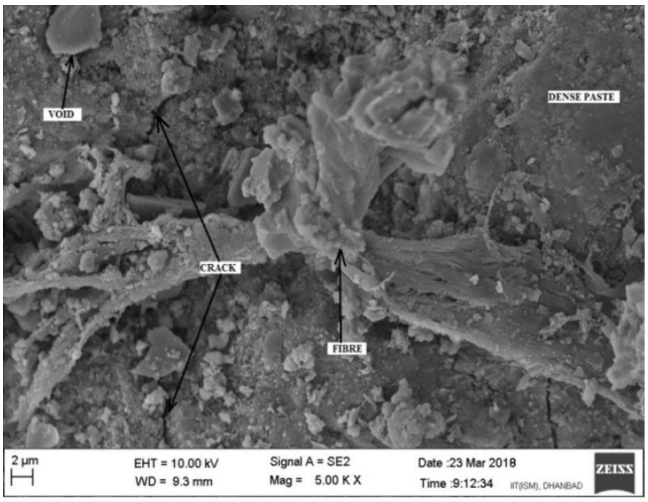



(**a**)



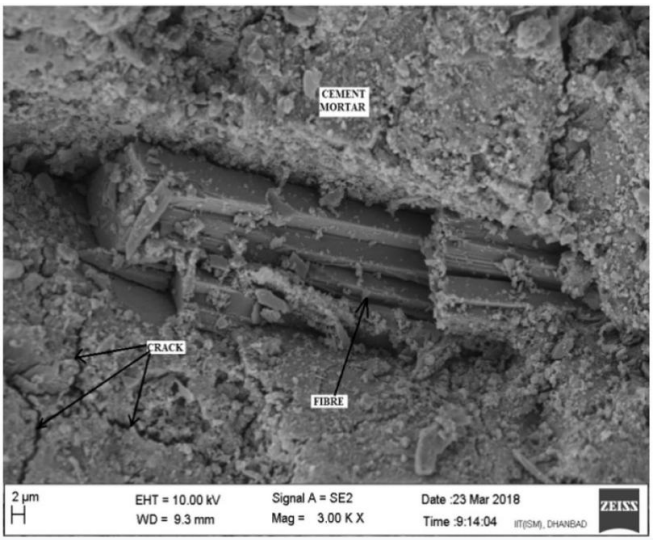

(**b**)

**Figure 22.** SEM images of the surfaces of RAC and NAC [121]. (**a**) RAC; (**b**) NAC.




(**a**)

**Figure 23.** *Cont.*

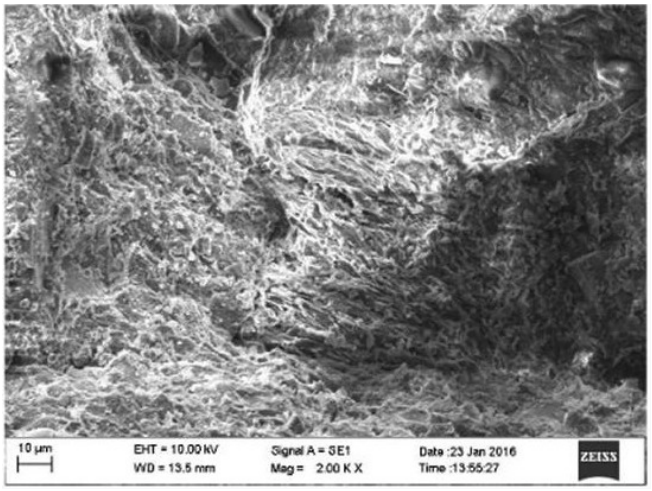



(**b**)

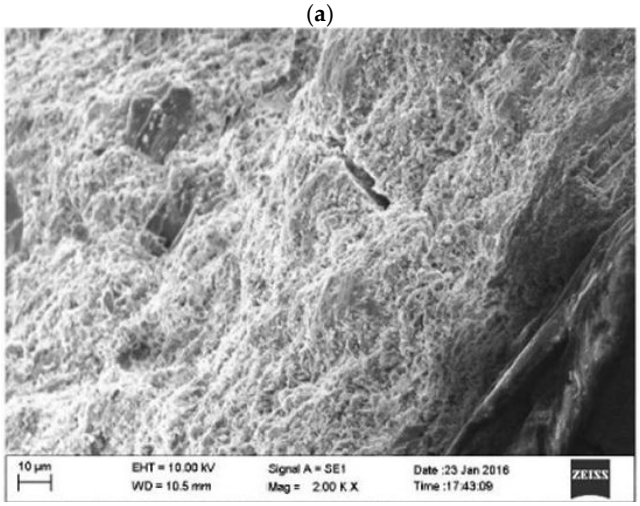
**Figure 23.** Field-emission SEM images of fibers in RAC [79]. (**a**) Bridging role of PP fibers (**b**) Fracture of PP fibers.

As shown in Figure 23, PP fibers played a bridging role in the matrix. There was a part of void between PP fibers and the matrix and the fracture of PP fibers, which negatively affected the performance of the matrix [79]. With the increasing of SF content, the number of cracks in the matrix decreased, but cracks still existed (Figure 24). This is because the cement mortar has a strong bond with the SFs, increasing the density of the matrix. However, the SFs could not undergo the hydration reaction, and there were still pores in the bond with the cement slurry. SFs can act as a bridge to prevent crack propagation. They can also transfer the heat of the cement hydration reaction, promote the cement hydration reaction, and make the ITZ denser [122].

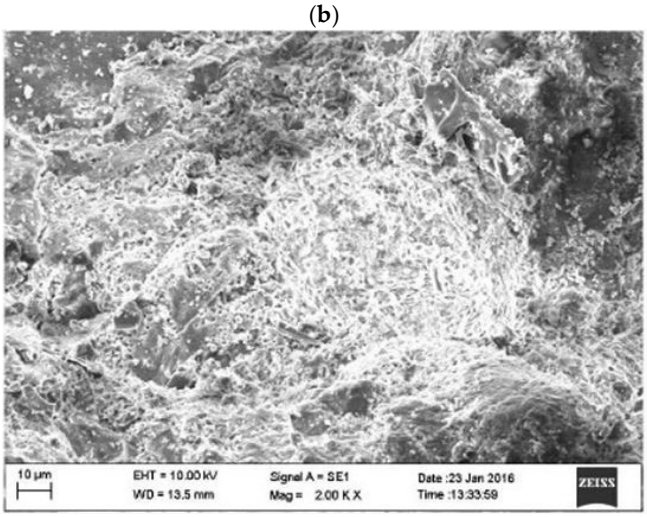
Xie et al. [70] found that when SF-doped RAC was heated to 200 °C, the moisture in the matrix evaporated, resulting in fine cracks. The ettringite began to decompose well below 400 °C. When the matrix was heated to 400 °C, the hydration products in the matrix were dehydrated, and Ca $(OH)_2$ began to decompose, resulting in mass loss and strength decline of the matrix. The C-S-H gel already dehydrates from 100 °C, reducing the density of the matrix. The calcium hydroxide began to decompose at 600 °C, generating calcium oxide, which absorbed moisture from the air, increasing the porosity of the concrete interior. At 800 °C, many cracks appeared in ITZs of the matrix. High temperature can reduce the compressive performance, elasticity modulus, and toughness of FRRAC. When silica fume, GGBS, MK or other mineral materials are mixed into the matrix, a pozzolanic reaction can occur, and the cementing substance C-S-H can be generated, improving the matrix performance. ITZ has a positive impact on the performance of the matrix. Moreover, adding appropriate fiber and mineral materials can improve the performance of the matrix. ITZ performance in RAC plays a decisive role in mechanical properties and durability. However, the performance of ITZ in RAC is worse than that of ordinary concrete. Therefore, proper amounts of PP fiber, SFs and mineral additive can be used to improve the ITZ performance of RAC.




(**a**)




(**b**)




(**c**)

**Figure 24.** Representative SEM images of Steel fiber-reinforced recycled coarse aggregate concrete (SFRCAC) [63]. (**a**) 0% SFs; (**b**) 1% SFs; (**c**) 2% SFs.

## 6. Conclusions

The research progress of PP fiber- and/or SFs-reinforced RAC was reviewed with a focus on its consistence, mechanical properties, durability, and microstructure. The following conclusions are drawn.

(1) The pozzolanic and filling effects of FA, GGBS, RHA, and silica fume can enhance the matrix compactness, improving the mechanical properties and durability of the matrix.
(2) RA is characterized by porosity and high water absorption; thus, the properties of RAC are poor. The addition of PP fibers and SFs to RAC can reduce the consistence of the matrix. The addition of SFs increased the compressive strength of RAC by 5.85–19%. However, in some studies, adding SFs reduced the compressive strength of the matrix, possibly owing to the shape and property of the SFs. Appropriate addition of SF and PP fibers can improve the RAC mechanical properties, but the excessive addition of fibers can degrade the mechanical properties of the matrix.
(3) The addition of RA can improve the performance of the matrix with regard to chloride-ion corrosion, and mass loss rate in freeze–thaw cycling. Appropriate addition of SFs and PP fibers reduces the RAC chloride-ions corrosion performance. Adding 5% air to RAC can yield the same durability as the NAC. After 300 freeze–thaw cycles, the mass loss of a matrix with 1% SF and 50% RA was only 0.2%. The matrix shrinkage can be reduced by adding SF and PP fibers.
(4) There are many pores and cracks in the ITZs of the RA matrix; thus, the RAC strength is lower than the NAC strength. Adding appropriate amounts of PP fibers and SFs can improve the ITZ compactness and delay the crack propagation, improving the mechanical properties and durability of the composite. The density of the matrix in the ITZs determines the mechanical properties of the matrix.

**Author Contributions:** Conceptualization, P.Z., Y.Y. and J.W.; formal analysis, P.Z., Y.Y., J.W., S.H.; resources, S.H.; writing—original draft preparation, P.Z., Y.Y., and J.W.; writing—review and editing, Y.Y., S.H., M.J. and Y.L.; supervision, M.J.; project administration, J.W.; funding acquisition, P.Z. All authors have read and agreed to the published version of the manuscript.

**Funding:** This research was funded by Open Projects Funds of Dike Safety and Disaster Prevention Engineering Technology Research Center of Chinese Ministry of Water Resources (Grant no. 2016001), National Natural Science Foundation of China (No. 51979251), Program for Innovative Research Team (in Science and Technology) in University of Henan Province of China (No. 20IRTSTHN009), Open Research Fund of State Key Laboratory of Simulation and Regulation of Water Cycle in River Basin (China Institute of Water Resources and Hydropower Research) (No. IWHR-SKL-201512). Innovation Group Science Foundation of the Natural Science Foundation of Chongqing, China (Grant no. cstc2020jcyj-cxttX0003).

**Conflicts of Interest:** The authors declare no conflict of interest.

## References

1. Tsai, C.Y.; Chang, A.S. Framework for developing construction sustainability items: The example of highway design. *J. Clean. Prod.* **2012**, *20*, 127–136. [CrossRef]
2. Khtar, A.A.; Sarmah, A.K. Construction and demolition waste generation and properties of recycled aggregate concrete: A global perspective. *J. Clean. Prod.* **2018**, *186*, 262–281. [CrossRef]
3. Wang, J.Y.; Li, Z.D.; Tam, V.W.Y. Critical factors in effective construction waste minimization at the design stage: A Shenzhen case study, China. *Resour. Conserv. Recycl.* **2014**, *82*, 1–7. [CrossRef]
4. Ahmed, W.; Lim, C.W. Production of sustainable and structural fiber reinforced recycled aggregate concrete with improved fracture properties: A review. *J. Clean. Prod.* **2021**, *279*, 123832. [CrossRef]
5. Jiménez, J.R.; Ayuso, J.; Galvín, A.P.; López, M.; Agrela, F. Use of mixed recycled aggregates with a low embodied energy from non-selected CDW in unpaved rural roads. *Constr. Build. Mater.* **2012**, *34*, 34–43. [CrossRef]

6. Silva, R.V.; Brito, J.D.; Dhir, R.K. Properties and composition of recycled aggregates from construction and demolition waste suitable for concrete production. *Constr. Build. Mater.* **2014**, *65*, 201–217. [CrossRef]
7. Senaratne, S.; Gerace, D.; Mirza, O.; Tam, V.W.Y.; Kang, W.-H. The costs and benefits of combining recycled aggregate with steel fibers as a sustainable, structural material. *J. Clean. Prod.* **2016**, *112*, 2318–2327. [CrossRef]
8. Sim, J.; Park, C. Compressive strength and resistance to chloride ion penetration and carbonation of recycled aggregate concrete with varying amount of fly ash and fine recycled aggregate. *Waste Manag.* **2011**, *31*, 2352–2360. [CrossRef]
9. Martínez, I.; Etxeberria, M.; Pavón, D.E.N. Influence of demolition waste fine particles on the properties of recycled aggregate masonry mortar. *Int. J. Civ. Eng.* **2018**, *16*, 1213–1226. [CrossRef]
10. Yang, Y.F.; Han, L.H. Experimental behaviour of recycled aggregate concrete filled steel tubular columns. *J. Constr. Steel. Res.* **2006**, *62*, 1310–1324. [CrossRef]
11. Limbachiya, M.; Meddah, M.S.; Ouchagour, Y. Use of recycled concrete aggregate in fly-ash concrete. *Constr. Build. Mater.* **2012**, *27*, 439–449. [CrossRef]
12. Xiao, J.; Li, W.; Fan, Y.; Huang, X. An overview of study on recycled aggregate concrete in China (1996–2011). *Constr. Build. Mater.* **2012**, *31*, 364–383. [CrossRef]
13. Thomas, C.D.L.; Setién, J.; Polanco, J.; Alaejos, P.; De Juan, M.S. Durability of recycled aggregate concrete. *Constr. Build. Mater.* **2013**, *40*, 1054–1065. [CrossRef]
14. Evangelista, L.; Brito, J.D. Mechanical behavior of concrete made with fine recycled concrete aggregates. *Cem. Concr. Compos.* **2007**, *29*, 397–401. [CrossRef]
15. Huda, S.B.; Alam, M.S. Mechanical and freeze-thaw durability properties of recycled aggregate concrete made with recycled coarse aggregate. *J. Civ. Eng. Mang.* **2015**, *27*, 04015003. [CrossRef]
16. Wagih, A.M.; El-Karmoty, H.Z.; Ebid, M.; Okba, S.H. Recycled construction and demolition concrete waste as aggregate for structural concrete. *HBRC. J.* **2013**, *9*, 193–200. [CrossRef]
17. Ajdukiewicz, A.; Kliszczewicz, A. Influence of recycled aggregates on mechanical properties of hs/hpc. *Cem. Concr. Compos.* **2002**, *24*, 269–279. [CrossRef]
18. Rao, A.; Jha, K.N.; Misra, S. Use of aggregates from recycled construction and demolition waste in concrete. *Resour. Conserv. Rec.* **2007**, *50*, 71–81. [CrossRef]
19. Xiao, J.; Li, J.; Zhang, C. Mechanical properties of recycled aggregate concrete under uniaxial loading. *Cem. Concr. Res.* **2005**, *35*, 1187–1194. [CrossRef]
20. González-Fonteboa, B.; Martínez-Abella, F.; Diego, C.L.; Sindy, S.-P. Stress-strain relationship in axial compression for concrete using recycled saturated coarse aggregate. *Constr. Build. Mater.* **2011**, *25*, 2335–2342.
21. Gowda, G.G.; Rao, B.S.; Naik, S.M. Behaviour of recycled aggregate concrete on exposed to elevated temperature. *Int. J. Civ. Eng.* **2017**, *4*, 5–13. [CrossRef]
22. Gales, J.; Parker, T.; Cree, D.; Green, M. *Fire Performance of Sustainable Recycled Concrete Aggregates: Mechanical Properties at Elevated Temperatures and Current Research Needs*; Springer: New York, NY, USA, 2016; pp. 817–845.
23. Shi, C.; Li, Y.; Zhang, J.; Li, W.; Chong, L.; Xie, Z. Performance enhancement of recycled concrete aggregate—A review. *J. Clean. Prod.* **2016**, *112*, 466–472. [CrossRef]
24. Thomas, J.; Thaickavil, N.N.; Wilson, P.M. Strength and durability of concrete containing recycled concrete aggregates. *J. Build. Eng.* **2018**, *19*, 349–365. [CrossRef]
25. Prokopski, G.; Halbiniak, J. Interfacial transition zone in cementitious materials. *Cem. Concr. Res.* **2000**, *30*, 579–583. [CrossRef]
26. Poon, C.S.; Shui, Z.H.; Lam, L. Effect of microstructure of ITZ on compressive strength of concrete prepared with recycled aggregates. *Constr. Build. Mater.* **2004**, *18*, 461–468. [CrossRef]
27. Zaetang, Y.; Sata, V.; Wongsa, A.; Chindaprasirt, P. Properties of pervious concrete containing recycled concrete block aggregate and recycled concrete aggregate. *Constr. Build. Mater.* **2016**, *11*, 15–21. [CrossRef]
28. Carneiro, J.A.; Lima, P.R.L.; Leite, M.B.; Filho, R.D.T. Compressive stress-strain behavior of steel fiber reinforced-recycled aggregate concrete. *Cem. Concr. Compos.* **2014**, *46*, 65–72. [CrossRef]
29. Tabsh, S.W.; Abdelfatah, A.S. Influence of recycled concrete aggregates on strength properties of concrete. *Constr. Build. Mater.* **2009**, *23*, 163–167. [CrossRef]
30. Papatzani, S.; Paine, K. Construction, demolition and excavation waste management in EU / Greece and its potential use in concrete. *Fresenius Environ. Bull.* **2017**, *26*, 5572–5580.

31. Behera, M.; Bhattacharyya, S.; Minocha, A.; Deoliya, R.; Maiti, S.N. Recycled aggregate from C&D waste & its use in concrete—A breakthrough towards sustainability in construction sector: A review. *Constr. Build. Mater.* **2014**, *68*, 501–516.
32. Qin, Y.; Zhang, X.; Chai, J.; Xu, Z.; Li, S. Experimental study of compressive behavior of polypropylene-fiber-reinforced and polypropylene-fiber-fabric-reinforced concrete. *Constr. Build. Mater.* **2019**, *194*, 216–225. [CrossRef]
33. Qin, Y.; Zhang, X.W.; Chai, J.R. Damage performance and compressive behavior of early-age green concrete with recycled nylon fiber fabric under an axial load. *Constr. Build. Mater.* **2019**, *209*, 105–114. [CrossRef]
34. Wang, L.; Guo, F.; Yang, H.; Wang, Y.; Tang, S. Comparison of fly ash, PVA fiber, MgO and shrinkage-reducing admixture on the frost resistance of face slab concrete via pore structural and fractal analysis. *Fractals* **2020**. [CrossRef]
35. Radonjanin, V.; Malešev, M.; Marinković, S.; Al Malty, A.E.S. Green recycled aggregate concrete. *Constr. Build. Mater.* **2013**, *47*, 1503–1511. [CrossRef]
36. Fonteboa, B.G.; Abella, F.M. Concretes with aggregates from demolition waste and silica fume materials and mechanical properties. *Build. Environ.* **2008**, *3*, 3357–3363.
37. Kou, S.C.; Poon, C.S. Long-term mechanical and durability properties of recycled aggregate concrete prepared with the incorporation of fly ash. *Cem. Concr. Compos.* **2013**, *37*, 12–19. [CrossRef]
38. Rattanachu, P.; Toolkasikorn, P.; Tangchirapat, W. Performance of recycled aggregate concrete with rice husk ash as cement binder. *Constr. Build. Mater.* **2020**, *108*, 103533. [CrossRef]
39. Majhi, R.K.; Nayak, A.N. Production of sustainable concrete utilising high-volume blast furnace slag and recycled aggregate with lime activator. *J. Clean. Prod.* **2020**, *255*, 120188. [CrossRef]
40. Nuaklong, P.; Sata, V.; Chindaprasirt, P. Properties of metakaolin-high calcium fly ash geopolymer concretecontaining recycled aggregate from crushed concrete specimens. *Constr. Build. Mater.* **2018**, *167*, 365–373. [CrossRef]
41. Koushkbaghi, M.; Kazemi, M.J.; Mosavietal, H. Acid resistance and durability properties of steel fiber-reinforced concrete incorporating rice husk ash and recycled aggregate. *Constr. Build. Mater.* **2019**, *202*, 266–275. [CrossRef]
42. Ali, B.; Qureshi, L.A.; Shah, S.H.A.; Rehman, S.U.; Hussain, I.; Iqbal, M. A step towards durable, ductile and sustainable concrete: Simultaneous incorporation of recycled aggregates, glass fiber and fly ash. *Constr. Build. Mater.* **2020**, *251*, 118980. [CrossRef]
43. Kim, K.; Shin, M.; Cha, S. Combined effects of recycled aggregate and fly ash towards concrete sustainability. *Constr. Build. Mater.* **2013**, *48*, 499–507. [CrossRef]
44. Padhi, R.S.; Patra, R.K.; Mukharjee, B.B.; Dey, T. Influence of incorporation of rice husk ash and coarse recycled concrete aggregates on properties of concrete. *Constr. Build. Mater.* **2018**, *10*, 289–297. [CrossRef]
45. Tangchirapat, W.; Buranasing, R.; Jaturapitakkul, C. Influence of rice husk-bark ash on mechanical properties of concrete containing high amount of recycled aggregates. *Constr. Build. Mater.* **2008**, *22*, 1812–1819. [CrossRef]
46. Alnahhal, M.F.; Alengaram, U.J.; Jumaat, M.Z.; AbuTaha, F.; Alqedra, M.A.; Nayaka, R.R. Assessment on engineering properties and $CO_2$ emissions of recycled aggregate concrete incorporating waste products as supplements to Portland cement. *J. Clean. Prod.* **2018**, *203*, 822–835. [CrossRef]
47. Corinaldesi, V.; Moriconi, G. Influence of mineral additions on the performance of 100% recycled aggregate concrete. *Constr. Build. Mater.* **2009**, *23*, 2869–2876. [CrossRef]
48. Koua, S.C.; Poon, C.S.; Agrelab, F. Comparisons of natural and recycled aggregate concretes prepared with the addition of different mineral admixtures. *Cem. Concr. Compos.* **2011**, *33*, 788–795. [CrossRef]
49. Çakır, Ö.; Sofyanlı, Ö.Ö. Influence of silica fume on mechanical and physical properties of recycled aggregate concrete. *HBRC J.* **2015**, *11*, 157–166. [CrossRef]
50. Pedro, D.; de Brito, J.; Evangelista, L. Mechanical characterization of high performance concrete prepared with recycled aggregates and silica fume from precast industry. *J. Clean. Prod.* **2017**, *164*, 939–949. [CrossRef]
51. Majhi, R.K.; Nayak, A.N.; Mukharjee, B.B. Development of sustainable concrete using recycled coarse aggregate and ground granulated blast furnace slag. *Constr. Build. Mater.* **2018**, *159*, 417–430. [CrossRef]
52. Majhi, R.K.; Nayak, A.N. Bond, durability and microstructural characteristics of ground granulated blast furnace slag based recycled aggregate concrete. *Constr. Build. Mater.* **2019**, *212*, 578–595. [CrossRef]

53. Muduli, R.; Mukharjee, B.B. Effect of incorporation of metakaolin and recycled coarse aggregate on properties of concrete. *J. Clean. Prod.* **2019**, *209*, 398–414. [CrossRef]
54. Xie, J.; Zhang, H.; Duan, L.; Yang, Y.; Yan, J.; Shan, D.; Liu, X.; Pang, J.; Chen, Y.; Li, X.; et al. Effect of nano metakaolin on compressive strength of recycled concrete. *Constr. Build. Mater.* **2020**, *256*, 119393. [CrossRef]
55. Juan, M.S.; Gutiérrez, P.A. Study on the influence of attached mortar content on the properties of recycled concrete aggregate. *Constr. Build. Mater.* **2009**, *23*, 872–877. [CrossRef]
56. Sun, C.; Chen, Q.; Xiao, J.; Liu, W. Utilization of waste concrete recycling materials in self-compacting concrete. *Res. Cons. Rec.* **2020**, *161*, 104930. [CrossRef]
57. Grdic, Z.J.; Toplicic-Curcic, G.A.; Despotovic, I.M.; Ristic, N.S. Properties of self-compacting concrete prepared with coarse recycled concrete aggregate. *Constr. Build. Mater.* **2010**, *24*, 1129–1133. [CrossRef]
58. Matar, P.; Assaad, J.J. Concurrent effects of recycled aggregates and polypropylene fibers on workability and key strength properties of self-consolidating concrete. *Constr. Build. Mater.* **2017**, *199*, 492–500. [CrossRef]
59. Akça, K.R.; Çakır, O.; Ipek, M. Properties of polypropylene fiber reinforced concrete using recycled aggregates. *Constr. Build. Mater.* **2015**, *98*, 620–630. [CrossRef]
60. Yazıcı, S.; Inan, G.; Tabak, V. Effect of aspect ratio and volume fraction of steel fiber on the mechanical properties of SFRC. *Constr. Build. Mater.* **2007**, *21*, 1250–1253. [CrossRef]
61. Gao, D.Y.; Zhang, L. Flexural performance and evaluation method of steel fiber reinforced recycled coarse aggregate concrete. *Constr. Build. Mater.* **2018**, *159*, 126–136. [CrossRef]
62. Mohseni, E.; Saadati, R.; Kordbacheh, N.; Parpinchi, Z.S.; Tang, W. Engineering and microstructural assessment of fiber-reinforced self-compacting concrete containing recycled coarse aggregate. *J. Clean. Prod.* **2017**, *168*, 605–613. [CrossRef]
63. Gao, D.; Zhang, L.; Zhao, J.; You, P. Durability of steel fiber-reinforced recycled coarse aggregate concrete. *Constr. Build. Mater.* **2020**, *232*, 117119. [CrossRef]
64. Kachouh, N.; Hassan, H.E.; Maaddawy, T.E. Effect of steel fibers on the performance of concrete made with recycled concrete aggregates and dune sand. *Constr. Build. Mater.* **2019**, *213*, 348–359. [CrossRef]
65. Hanumesh, B.M.; Harish, B.A.; Ramana, N.V. Influence of polypropylene fibers on recycled aggregate concrete. *Mater. Today.* **2018**, *5*, 1147–1155.
66. Hossain, F.Z.; Shahjalal, M.; Islam, K.; Tiznobaik, M.; Alam, M.S. Mechanical properties of recycled aggregate concrete containing crumb rubber and polypropylene fiber. *Constr. Build. Mater.* **2019**, *225*, 983–996. [CrossRef]
67. Choi, W.C.; Yun, H.D. Compressive behavior of reinforced concrete columns with recycled aggregate under uniaxial loading. *Eng. Struct.* **2012**, *41*, 285–293. [CrossRef]
68. Ahmed, T.W.; Mali, A.A.; Zidan, R.S. Properties of high strength polypropylene fiber concrete containing recycled aggregate. *Constr. Build. Mater.* **2020**, *241*, 118010. [CrossRef]
69. Afroughsabet, V.; Biolzi, L.; Ozbakkaloglu, T. Influence of double hooked-end steel fibers and slag on mechanical and durability properties of high performance recycled aggregate concrete. *Compos. Struct.* **2017**, *181*, 273–284. [CrossRef]
70. Xie, J.; Zhang, Z.; Lu, Z.; Sun, M. Coupling effects of silica fume and steel-fiber on the compressive behaviour of recycled aggregate concrete after exposure to elevated temperature. *Constr. Build. Mater.* **2018**, *184*, 752–764. [CrossRef]
71. Wang, L.; Jin, M.; Guo, F.; Wang, Y.; Tang, S. Pore structural and fractal analysis of the influence of fly ash and silica fume on the mechanical property and abrasion resistance of concrete. *Fractals* **2020**. [CrossRef]
72. Wang, L.; Luo, R.; Zhang, W.; Jin, M.; Tang, S. Effects of fineness and content of phosphorus slag on cement hydration, permeability, pore structure and fractal dimension of concrete. *Fractals* **2020**. [CrossRef]
73. Saad, M.; Abo-El-Enein, S.A.; Hanna, G.B.; Kotkata, M.F. Effect of temperature on physical and mechanical properties of concrete containing silica fume. *Cem. Concr. Compos.* **1996**, *26*, 669–675. [CrossRef]
74. Ahmadia, M.; Farzin, S.; Hassanib, A.; Motamedia, M. Mechanical properties of the concrete containing recycled fiber and aggregates. *Constr. Build. Mater.* **2017**, *144*, 392–398. [CrossRef]
75. He, W.; Kong, X.; Fu, Y.; Zhou, C.; Zheng, Z. Experimental investigation on the mechanical properties and microstructure of hybrid fiber reinforced recycled aggregate concrete. *Constr. Build. Mater.* **2020**, *261*, 12048. [CrossRef]

76. Yao, W.; Li, J.; Wu, K. Mechanical properties of hybrid fiber-reinforced concrete at low fiber volume fraction. *Cem. Concr. Compos.* **2003**, *33*, 27–30. [CrossRef]
77. Xu, F.; Wang, S.; Li, T.; Liu, B.; Li, B.; Zhou, Y. Mechanical properties and pore structure of recycled aggregate concrete made with iron ore tailings and polypropylene fibers. *J. Build. Eng.* **2021**, *33*, 101572. [CrossRef]
78. Zhang, S.P.; He, P.L.; Niu, L.L. Mechanical properties and permeability of fiber-reinforced concrete with recycled aggregate made from waste clay brick. *J. Clean. Prod.* **2020**, *268*, 121690. [CrossRef]
79. Das, C.S.; Dey, T.; Dandapat, R.; Mukharjee, B.B.; Kumar, J. Performance evaluation of polypropylene fiber reinforced recycled aggregate concrete. *Constr. Build. Mater.* **2018**, *189*, 649–659. [CrossRef]
80. Berredjem, L.; Arabi, N.; Molez, L. Mechanical and durability properties of concrete based on recycled coarse and fine aggregates produced from demolished concrete. *Constr. Build. Mater.* **2020**, *246*, 118421. [CrossRef]
81. Poon, C.S.; Shui, Z.H.; Lam, L. Compressive behavior of fiber reinforced high-performance concrete subjected to elevated temperatures. *Cem. Concr. Res.* **2004**, *34*, 2215–2222. [CrossRef]
82. Wang, Y.; Zhang, H.; Geng, Y.; Wang, Q.; Zhang, S. Prediction of the elastic modulus and the splitting tensile strength of concrete incorporating both fine and coarse recycled aggregate. *Constr. Build. Mater.* **2019**, *215*, 332–346. [CrossRef]
83. Deb, P.S.; Nat, P.H.; Sarker, P.K. The effects of ground granulated blast-furnace slag blending with fly ash and activator content on the workability and strength properties of geopolymer concrete cured at ambient temperature. *Mater. Design.* **2014**, *62*, 32–39. [CrossRef]
84. Çakır, Ö. Experiment alanalysis of properties of recycled coarse aggregate (RCA) concrete with mineral additives. *Constr. Build. Mater.* **2014**, *68*, 17–25. [CrossRef]
85. Duan, Z.H.; Poon, C.S. Properties of recycled aggregate concrete made with recycled aggregates with different amounts of old adhered mortars. *Mater. Design.* **2014**, *58*, 19–29. [CrossRef]
86. Ismail, S.; Kwan, W.H.; Ramli, M. Mechanical strength and durability properties of concrete containing treated recycled concrete aggregates under different curing conditions. *Constr. Build. Mater.* **2017**, *155*, 296–306. [CrossRef]
87. Nepomuceno, M.C.S.; Isidoro, R.A.S.; Catarino, J.P.G. Mechanical performance evaluation of concrete made with recycled ceramic coarse aggregates from industrial brick waste. *Constr. Build. Mater.* **2018**, *165*, 284–294. [CrossRef]
88. Yoo, D.; Yoon, Y.; Banthia, N. Flexural response of steel-fiber-reinforced concrete beams: Effects of strength, fiber content, and strain-rate. *Cem. Concr. Compos.* **2015**, *64*, 84–92. [CrossRef]
89. Yoo, D.; Banthia, N.; Kang, S.; Yoon, Y. Effect of fiber orientation on the rate dependent flexural behavior of ultra-high-performance fiber-reinforced concrete. *Compos. Struct.* **2016**, *157*, 62–70. [CrossRef]
90. Abdallah, S.; Rees, D.W.A.; Ghaffar, S.H.; Fan, M. Understanding the effects of hooked-end steel fibre geometry on the uniaxial tensile behaviour of self-compacting concrete. *Constr. Build. Mater.* **2018**, *178*, 484–494. [CrossRef]
91. Kayali, O.; Haque, M.N.; Zhu, B. Some characteristics of high strength fiber reinforced lightweight aggregate concrete. *Cem. Concr. Compos.* **2003**, *25*, 207–213. [CrossRef]
92. Hughes, B.P.; Fattuhi, N.I. Stress-strain curves for fiber reinforced concrete in compression. *Cem. Concr. Res.* **1977**, *7*, 173–184. [CrossRef]
93. Cachim, P.B.; Figueiras, J.; Pereira, P.A. Fatigue behavior of fiber-reinforced in compression. *Cem. Concr. Compos.* **2002**, *24*, 211–217. [CrossRef]
94. Ramesh, K.; Seshu, D.R.; Prabhakar, M. Constitutive behaviour of confined fiber reinforced concrete under axial compression. *Cem. Concr. Compos.* **2003**, *25*, 343–350. [CrossRef]
95. *GB50081-2002. Standard for Test Method of Mechanical Properties on Ordinary Concrete*; National Standard of the People's Republic of China: Beijing, China, 2003.
96. Xie, J.H.; Guo, Y.C.; Liu, L.S.; Xie, Z.H. Compressive and flexural behaviors of a new steel-fiber-reinforced recycled aggregate concrete with crumb rubber. *Constr. Build. Mater.* **2015**, *79*, 263–272. [CrossRef]
97. Sato, R.; Maruyama, I.; Sogabe, T.; Sogo, M. Flexural behavior of reinforced recycled concrete beams. *J. Adv. Concr. Technol.* **2007**, *5*, 43–61. [CrossRef]
98. Wong, H.; Zobel, M.; Buenfeld, N.; Zimmerman, R. Influence of the interfacial transition zone and microcracking on the diffusivity, permeability and sorptivity of cement-based materials after drying. *Mag. Concr. Res.* **2009**, *61*, 571–589. [CrossRef]

99. Guo, Y.C.; Zhang, J.H.; Chen, G.M.; Xie, Z.H. Compressive behavior of concrete structures incorporating recycled concrete aggregates, rubber crumb and reinforced with steel fiber, subjected to elevated temperatures. *J. Clean. Prod.* **2014**, *72*, 193–203. [CrossRef]
100. Reddy, D.V.; Pawade, P.Y. Combine effect of silica fume and steel fiber on mechanical properties on standard grade of concrete and their interrelations. *Int. J. Adv. Manuf. Tech.* **2012**, *94*, 361–366.
101. Chen, G.M.; He, Y.H.; Yang, H.; Chen, J.F.; Guo, Y. Compressive behavior of steel fiber reinforced recycled aggregate concrete after exposure to elevated temperatures. *Constr. Build. Mater.* **2014**, *71*, 1–15. [CrossRef]
102. Mansour, H.B.; Dhouibi, L.; Idrissi, H. Effect of phosphate-based inhibitor on prestressingtendons corrosion in simulated concrete pore solution contaminated by chlorideions. *Constr. Build. Mater.* **2018**, *171*, 250–260. [CrossRef]
103. Jung, M.S.; Kim, K.B.; Lee, S.A.; Ann, K.Y. Risk of chloride-induced corrosion of steel in SF concrete exposed to a chloride-bearing environment. *Constr. Build. Mater.* **2018**, *166*, 413–422. [CrossRef]
104. Zhu, P.; Hao, Y.; Liu, H.; Wei, D.; Liu, S.; Gu, L. Durability evaluation of three generations of 100% repeatedly recycled coarse aggregate concrete. *Constr. Build. Mater.* **2019**, *210*, 442–450. [CrossRef]
105. Vieira, T.; Alves, A.; De Brito, J.; Correia, J.; Silva, R. Durability-related performance of concrete containing fine recycled aggregates from crushed bricks and sanitary ware. *Mater. Des.* **2016**, *90*, 767–776. [CrossRef]
106. Medina, C.; De Rojas, M.I.S.; Thomas, C.; Polanco, J.A.; Frias, M.F. Durability of recycled concrete made with recycled ceramic sanitary ware aggregate. Inter-indicator relationships. *Constr. Build. Mater.* **2016**, *105*, 480–486. [CrossRef]
107. Medina, C.; Rojas, M.F.; De Rojas, M.S.; Thomas, C.; Polanco, J.A.; De Rojas, M. Gas permeability in concrete containing recycled ceramic sanitary ware aggregate. *Constr. Build. Mater.* **2012**, *37*, 597–605. [CrossRef]
108. Zhan, B.J.; Poon, C.S.; Shi, C.J. $CO_2$ curing for improving the properties of concrete blocks containing recycled aggregates. *Cem. Concr. Compos.* **2013**, *42*, 1–8. [CrossRef]
109. Pan, H.; Yang, Z.; Xu, F. Study on concrete structure's durability considering the interaction of multi-factors. *Constr. Build. Mater.* **2016**, *118*, 256–261. [CrossRef]
110. Wang, C.; Xiao, J.; Zhang, G.; Li, L. Interfacial properties of modeled recycled aggregate concrete modified by carbonation. *Constr. Build. Mater.* **2016**, *105*, 307–320. [CrossRef]
111. Mehta, P.K.; Monteiro, P.J.P. *Concrete Microstructure, Properties and Material*; Mc Graw Hill: New York, NY, USA, 2006.
112. Tuyan, M.; Aghabaglou, A.M.; Ramyar, K. Freeze-thaw resistance, mechanical and transport properties of self-consolidating concrete incorporating coarse recycled concrete aggregate. *Mater. Design.* **2014**, *53*, 983–991. [CrossRef]
113. Richardson, A.; Coventry, K.; Bacon, J. Freeze/thaw durability of concrete with recycled demolition aggregate compared to virgin aggregate concrete. *J. Clean. Prod.* **2011**, *19*, 272–277. [CrossRef]
114. Šeps, K.; Fládr, J.; Broukalová, I. Resistance of recycled aggregate concrete to freeze-thaw and deicing salts. *Procedia Eng.* **2016**, *151*, 329–336. [CrossRef]
115. Kou, S.; Poon, C. Effect of the quality of parent concrete on the properties of high performance recycled aggregate concrete. *Constr. Build. Mater.* **2015**, *77*, 501–508. [CrossRef]
116. Domingo-Cabo, A.; Lázaro, C.; López-Gayarre, F.; Serrano-López, M.; Serna, P.; Castaño-Tabares, J. Creep and shrinkage of recycled aggregate concrete. *Constr. Build. Mater.* **2009**, *23*, 2545–2553. [CrossRef]
117. Corominas, A.G.; Etxeberria, M. Effects of using recycled concrete aggregates on the shrinkage of high performance concrete. *Constr. Build. Mater.* **2016**, *115*, 32–41. [CrossRef]
118. MesbahU, H.A.; Bodin, F.B. Efficiency of polypropylene and metallic fibers on control of shrinkage and cracking of recycled aggregate mortars. *Constr. Build. Mater.* **1999**, *13*, 439–447. [CrossRef]
119. Kaïkea, A.; Achoura, D.; Duplan, F.; Rizzuti, L. Effect of mineral admixtures and steel fiber volume contents on the behavior of high performance fiber reinforced concrete. *Mater. Design.* **2014**, *63*, 493–499. [CrossRef]
120. Bywalski, C.; Kaminski, M.; Maszczak, M. Influence of steel fibers addition on mechanical and selected rheological properties of steel fiber high-strength reinforced concrete. *Arch. Civ. Mech. Eng.* **2015**, *15*, 742–750. [CrossRef]

121. Kazmi, S.M.S.; Munir, M.J.; Wu, Y.-F.; Patnaikuni, I. Effect of macro-synthetic fibers on the fracture energy and mechanical behavior of recycled aggregate concrete. *Constr. Build. Mater.* **2018**, *189*, 857–868. [CrossRef]
122. Gao, D.Y.; Zhang, L.J.; Nokken, M. Compressive behavior of steel fiber reinforced recycled coarse aggregate concrete designed with equivalent cubic compressive strength. *Constr. Build. Mater.* **2017**, *141*, 235–244. [CrossRef]

**Publisher's Note:** MDPI stays neutral with regard to jurisdictional claims in published maps and institutional affiliations.



© 2020 by the authors. Licensee MDPI, Basel, Switzerland. This article is an open access article distributed under the terms and conditions of the Creative Commons Attribution (CC BY) license (http://creativecommons.org/licenses/by/4.0/).